CHEMISTRY
A European Journal

Supporting Information

Introducing LNAzo: More Rigidity for Improved Photocontrol of Oligonucleotide Hybridization**

Nikolai Grebenovsky, Larita Luma, Patricia Müller, and Alexander Heckel*[a]

chem_201903240_sm_miscellaneous_information.pdf

Table of content

1. Chemical synthesis

1.1 Devices and Materials

Conditions

If necessary, reactions were carried out under Schlenk conditions, which means only dry solvents stored over molecular sieve were used in oven-dried Schlenk glassware. Reactions were carried out under argon atmosphere to exclude moisture.

Solvent

Dry solvents were purchased from the company Acros and used without any further purification in the synthesis. If not otherwise stated, solvents of technical grade were used.

Reagents

All chemicals used were purchased from Sigma-Aldrich, Fluka, Alfa Aesar, TCI, ChemPur, Carbosynth or Fluorochem and used without any further purification in the synthesis.

NMR-Spectroscopy

The NMR spectra were measured on the devices AM 250, AV 300, AV400 and AV 500 from Bruker. As suitable solvents for the NMR sample DMSO-*d*6 (^{1}H, δ = 2:49 ppm, ^{13}C, δ = 39.52 ppm) and $CDCl_3$ (^{1}H, δ = 7.26 ppm, ^{13}C, δ = 77.16 ppm) were used. The chemical shift is given in ppm. The abbreviations of the multiplicity of the signals are as follows: singlet = s, doublet = d, triplet = t, quartet = q, quintet = qn, multiplet = m. Corresponding combinations are used deductively, for example, dt for doublet of triplets.

TLC

To check the reaction progress of all reactions, thin layer chromatography plates silica gel 60 F254 on aluminum foil from Macherey-Nagel were used. The evaluation was performed visually using a UV lamp having a wavelength of λ = 254 nm or 365 nm.

Column-Chromatography

Purification by using column chromatography was performed using silica gel 60 (particle size: 40-63 µm) from Macherey-Nagel and technical solvents.

Mass-Spectrometry

ESI-MS were measured on a VG Platform II Fisons and high resolution mass spectra were measured on a MALDI LTQ Orbitrap XL from Thermo Fisher Scientific. Mass spectra were measured by the MS service department of the Goethe University Frankfurt (Matthias Brandl, Andreas Münch, Uwe Hener and Simon Zenglein), who we would like thank for their work.
Oligonucleotide mass spectra were measured on a Bruker micrOTOF-Q device by Martin Held and Patricia Müller, who we would like to thank for their work.

1.2 Locked azobenzene *C*-nucleosides

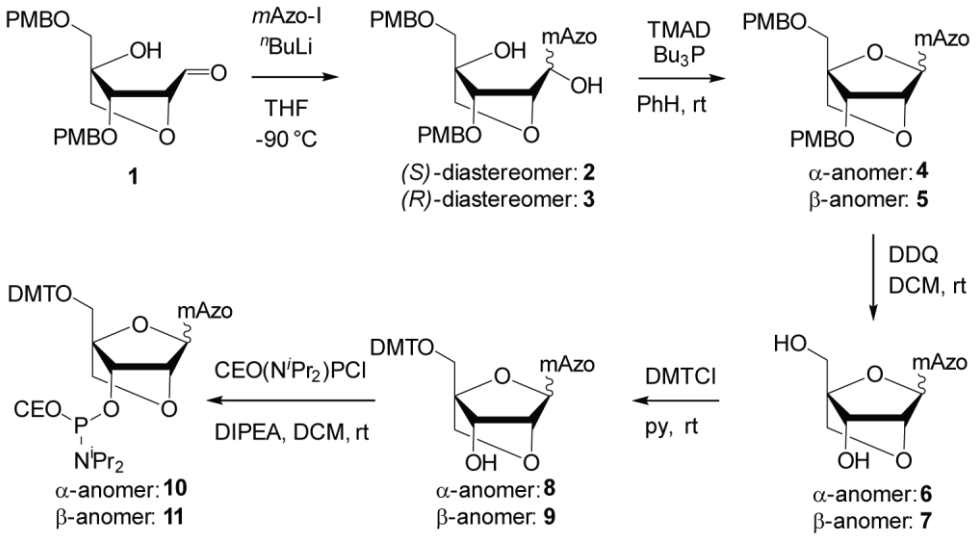

Figure S1: Synthetic approach to afford LNAzo-phosphoramidites used in this study.

(2*S*,3*S*,4*S*)-Hydroxy-2-[(*R*)-hydroxy-1'-(*m*-azobenzyl)methyl]-4-(*p*-methoxybenzyloxy)-3-(*p*-methoxybenzyloxymethyl)-tetrahydrofuran (**2**, **3**)

M-Iodoazobenzene (17.64 g, 57.29 mmol, 7.10 eq) was dissolved in 100.0 mL dry THF and cooled to -90 °C. *N*-Butyllithium (2.5 M in hexane, 22.6 mL, 59.98 mmol, 7.0 eq) was added dropwise while stirring vigorously. After 30 min. the solution was transferred to a solution of compound **1** (3.247 g, 8.069 mmol, 1.0 eq.) in 35.0 mL of dry THF at -90 °C and stirred for 1 h. The reaction was stopped by addition of aqueous NH_4Cl-solution. The organic phase was extracted with DCM, dried over Na_2SO_4 and evaporated to dryness. Crude product was subjected to flash column chromatography (Cy/EA + 1% TEA 2:1 → 1:1) and successive reverse phase column chromatography (MeOH:H_2O 4:1 → 9:1) for diastereomer separation to afford orange viscous oils as products.

(S)-diastereomer (**2**):

Yield: 0.654 g (1.119 mmol, 13%)
^{1}H-NMR (500 MHz, $CDCl_3$-*d*) δ 8.05 (s, 1H, Ar-H), 7.95 – 7.92 (m, 2H, Ar-H), 7.87 (d, *J* = 7.7 Hz, 1H, Ar-H), 7.60 – 7.45 (m, 5H, Ar-H), 7.25 – 7.19 (m, 2H, Ar-H), 6.90 – 6.83 (m, 2H, Ar-H), 6.71 (d, *J* = 8.8 Hz, 2H, Ar-H), 6.63 (d, *J* = 8.7 Hz, 2H, Ar-H), 5.20 (d, *J* = 2.9 Hz, 1H, 1'-H), 4.49 (s, 2H, CH_2), 4.29 – 4.27 (m, 1H, 2'-H), 3.95 (d, *J* = 9.4 Hz, 1H, CH_2), 3.84 (d, *J* = 1.3 Hz, 1H, 3'-H), 3.79 (s, 4H, CH_2+Ar-OMe), 3.75 – 3.70 (m, 3H, CH_2+CH_2), 3.66 (s, 3H, Ar-OMe), 3.52 (d, *J* = 9.4 Hz, 1H, CH_2).
^{13}C-NMR (126 MHz, $CDCl_3$-*d*) δ 159.6, 159.2, 153.0, 152.7, 142.1, 131.3, 129.8, 129.3, 129.3, 128.7, 123.1, 122.3, 120.6, 114.0, 113.7, 90.9, 81.9, 81.4, 73.1, 71.3, 68.8, 55.4, 55.2.
TLC (Cy:EA 1:1) R_f = 0.52.
HRMS (MALDI) $[M+H]^+$ m/z = calculated: 585.25953, found: 585.25759.

(*R*)-diastereomer (**3**):

Yield: 0.332 g (0.568 mmol, 7%)
^{1}H-NMR (500 MHz, $CDCl_3$-*d*) δ 7.93 (dd, *J* = 7.1, 1.3 Hz, 3H, Ar-H), 7.87 (dt, *J* = 7.5, 1.6 Hz, 1H, Ar-H), 7.58 – 7.44 (m, 5H, Ar-H), 7.28 – 7.19 (m, 2H, Ar-H), 6.93 (d, *J* = 8.6 Hz, 2H, Ar-H), 6.88 (d, *J* = 8.6 Hz, 2H, Ar-H), 6.74 (d, *J* = 8.7 Hz, 2H, Ar-H), 4.85 (d, *J* = 6.0 Hz, 1H, 1'-H), 4.51 (s, 2H, CH_2), 4.20 (d, *J* = 5.9 Hz, 1H, 2'-H), 4.15 (dd, *J* = 6.0, 2.3 Hz, 1H, CH_2), 3.92 (d, *J* = 9.4 Hz, 1H, CH_2), 3.80 (s, 6H, CH_2+3'-H, Ar-OMe), 3.76 (d, *J* = 9.3 Hz, 1H, CH_2), 3.71 (s, 3H, Ar-OMe), 3.53 (d, *J* = 9.3 Hz, 1H, CH_2).
^{13}C-NMR (126 MHz, $CDCl_3$-*d*) δ 159.5, 159.4, 152.8, 152.7, 142.2, 131.2, 129.7, 129.6, 129.3, 129.2, 114.0, 113.9, 89.3, 84.4, 81.9, 75.4, 74.4, 73.6, 71.9, 69.1, 55.4, 55.3.
TLC (Cy:EA 1:1) R_f = 0.39.
HRMS (MALDI) $[M+H]^+$ m/z = calculated: 585.25953, found: 585.23724

(1*S*,3*S*,4*R*,7*S*)-1'-(*m*-Azobenzyl)-7-(*p*-methoxybenzyloxy)-1-(*p*-methoxybenzyloxymethyl)-2,5-dioxabicyclo[2.2.1]heptane (**4**, **5**)

Tetramethylazodicarboxamide (0.289 g, 1.679 mmol, 1.5 eq / 0.148 g, 0.852 mmol, 1.5 eq) was dissolved in 10.0 mL dry benzene at 0 °C. Tributylphosphine (0.340 g, 1.679 mmol, 1.5 eq / 0.172 g, 0.852 mmol, 1.5 eq) and compound **2** or **3** (0.654 g, 1.119 mmol, 1.0 eq / 0.332 g, 0.568 mmol, 1.0 eq) dissolved in 1.0 mL dry benzene were added successively and stirred at room temperature overnight. The reaction was stopped by pouring into an aqueous NH_4Cl-solution. The organic phase was extracted with DCM, dried over Na_2SO_4 and evaporated to dryness. The crude product was subjected to flash column chromatography (Cy:EA + 1% TEA 4:1 → 1:1) to afford the product as viscous orange oil.

α-anomer (**4**):

Yield: 0.606 g (1.069 mmol, 96%)
^{1}H-NMR (500 MHz, $CDCl_3$-*d*) δ 7.93 – 7.89 (m, 3H, Ar-H), 7.86 – 7.82 (m, 1H, Ar-H), 7.54 – 7.46 (m, 5H, Ar-H), 7.32 – 7.27 (m, 4H, Ar-H), 6.92 – 6.85 (m, 5H, Ar-H), 5.26 (s, 1H, 1'-H), 4.67 – 4.56 (m, 4H, CH_2+CH_2), 4.43 (s, 1H, 2'-H), 4.32 (s, 1H, 3'-H), 4.04 – 3.98 (m, 1H, CH_2), 3.82 (s, 3H, Ar-OMe), 3.81 (s, 3H, Ar-OMe), 3.83 – 3.72 (m, 1H, CH_2).
^{13}C-NMR (126 MHz, $CDCl_3$-*d*) δ 159.5, 152.8, 140.1, 131.1, 129.8, 129.6, 129.5, 129.2, 129.1, 123.0, 122.2, 120.7, 114.0, 114.0, 87.6, 82.1, 80.8, 73.6, 71.8, 65.8, 55.4, 55.4.
TLC (Cy:EA 1:1) R_f = 0.50.
HRMS (MALDI) $[M+H]^+$ m/z = calculated: 567.24896, found: 567.24702.

β-anomer (**5**):

Yield: 0.239 g (0.422 mmol, 74%)
^{1}H-NMR (500 MHz, $CDCl_3$-*d*) δ 7.94 – 7.90 (m, 2H, Ar-H), 7.90 – 7.87 (m, 1H, Ar-H), 7.82 (d, *J* = 7.9 Hz, 1H, Ar-H), 7.55 – 7.46 (m, 4H, Ar-H), 7.32 – 7.29 (m, 2H, Ar-H), 7.12 – 7.09 (m, 2H, Ar-H), 6.88 (dd, *J* = 10.8, 8.2 Hz, 3H, Ar-H), 6.78 – 6.73 (m, 2H, Ar-H), 5.26 (s, 1H, 1'-H), 4.60 (dd, *J* = 19.6, 8.4 Hz, 2H, CH_2), 4.47 – 4.42 (m, 1H, CH_2), 4.37 (d, *J* = 11.3 Hz, 1H, CH_2), 4.25 (s, 1H, 2'-H), 4.11 (d, *J* = 1.4 Hz, 1H, CH_2), 4.04 (s, 1H, 3'-H), 3.85 (dd, *J* = 23.4, 11.5 Hz, 2H, CH_2), 3.78 (s, 3H, Ar-OMe), 3.73 (s, 3H, Ar-OMe).^{13}C-NMR (126 MHz, $CDCl_3$-*d*) δ 159.4, 159.3, 152.9, 152.7, 140.7, 131.3, 130.3, 129.6, 129.4, 129.3, 128.0, 123.1, 123.0, 121.8, 120.2, 113.9, 113.9, 86.2, 83.8, 72.0, 66.3, 55.4.
TLC (Cy:EA 1:1) R_f = 0.71.
HRMS (MALDI) $[M+H]^+$ m/z = calculated: 567.24896, found: 567.24634.

(1*S*,3*S*,4*R*,7*S*)-1'-(*m*-azobenzyl)-7-hydroxy-1-hydroxymethyl-2,5-dioxabicyclo[2.2.1]heptane (**6**, **7**)

Compound **4** (0.606 g, 1.069 mmol, 1.0 eq) or **5** (0.239 g, 0.422 mmol, 1.0 eq) was dissolved in 10.0 mL DCM. Upon addition of 0.5 mL water and DDQ (0.335 g, 1.476 mmol, 3.5 eq / 0.850 g, 3,743 mmol, 3.5 eq) the reaction was left to stir over night. The reaction was filtered, the organic phase washed with an aqueous $NaHCO_3$ solution and brine successively, dried over Na_2SO_4 and evaporated to dryness. The crude product was subjected to flash column chromatography (DCM:MeOH 19:1 → 9:1) to afford the product as viscous orange oil.

α-anomer (**6**):

Yield: 0.221 g (0,677 mmol, 63%)
^{1}H-NMR (400 MHz, DMSO-d_6) δ 7.96 – 7.88 (m, 3H, Ar-H), 7.79 (dq, *J* = 7.0, 2.8, 2.2 Hz, 1H, Ar-H), 7.64 – 7.55 (m, 5H, Ar-H), 5.62 (d, *J* = 4.3 Hz, 1H, 3'-OH), 5.27 (s, 1H, 1'-H), 4.84 (t, *J* = 5.7 Hz, 1H, 5'-OH), 4.30 – 4.24 (m, 2H, 2'-H+3'-H), 3.86 (d, *J* = 7.6 Hz, 1H, 6'-H), 3.76 (t, *J* = 6.9 Hz, 3H, 6'-H+5'-CH_2).
^{13}C-NMR (126 MHz, $CDCl_3$) δ 152.8, 152.8, 139.7, 131.2, 129.3, 128.4, 123.0, 122.3, 120.5, 88.3, 81.9, 81.7, 72.7, 58.9.
TLC (Cy:EA 1:1) R_f = 0.52.
HRMS (MALDI) $[M+H]^+$ m/z = calculated: 327.13393, found: 327.13383.

β-anomer (**7**):

Yield: 0.078 g (0,239 mmol, 57%)
^{1}H-NMR (400 MHz, DMSO-d_6) δ 7.94 – 7.88 (m, 3H, Ar-H), 7.77 (dt, *J* = 6.5, 2.2 Hz, 1H, Ar-H), 7.65 – 7.55 (m, 5H, Ar-H), 5.35 (d, *J* = 4.4 Hz, 1H, 3'-OH), 5.08 (s, 1H, 1'-H), 4.95 (t, *J* = 5.7 Hz, 1H, 5'-OH), 4.15 (s, 1H, 2'-H), 3.94 (d, *J* = 4.3 Hz, 1H, 3'-H), 3.91 (d, *J* = 7.5 Hz, 1H, 6'-H), 3.81 (d, *J* = 7.5 Hz, 1H, 6'-H), 3.78 (dd, *J* = 5.7, 1.9 Hz, 2H, 5'-CH_2).
^{13}C-NMR (126 MHz, $CDCl_3$) δ 152.9, 152.7, 139.9, 131.4, 129.6, 129.3, 127.8, 123.1, 122.4, 119.8, 86.8, 83.9, 83.3, 72.5, 71.7, 59.6.
TLC (Cy:EA 1:1) R_f = 0,44.
HRMS (MALDI) $[M+H]^+$ m/z = calculated: 327.13393, found: 327.13374.

(1*R*,3*S*,4*R*,7*S*)-1-(4,4‘-Dimethoxytrityloxymethyl)-1‘-(*m*-azobenzyl)-3-hydroxy-2,4-dioxabicyclo[2.2.1]heptane (**8**, **9**)

Compounds **6** (0.078 g, 0,239 mmol, 1.0 eq) or **7** (0.221 g, 0,677 mmol, 1.0 eq) were dissolved in 5.0 mL dry pyridine. DMTCl (0.089 g, 0.262 mmol, 1.1 eq / 0.221 g, 0.745 mmol, 1.1 eq) dissolved in 5.0 mL of dry pyridine was added dropwise over a time of 45 min. at 0 °C and left to stir for 4 h. Upon completion of the reaction, pyridine was coevaporated with toluene. The residue was extracted with DCM, the organic layer was dried over Na_2SO_4 and evaporated to dryness. The crude product was subjected to flash column chromatography (Cy:EA 2:1 + 1% TEA → EA:MeOH 9:1) to afford the product as orange foam.

α-anomer (**8**):

Yield: 0.195 g (0.310 mmol, 46%).
^{1}H-NMR (500 MHz, DMSO-*d*$_6$) δ 8.01 (s, 1H, Ar-H), 7.92 – 7.88 (m, *J* = 8.1, 1.5 Hz, 2H, Ar-H), 7.85 – 7.82 (m, 1H, Ar-H), 7.66 – 7.57 (m, 5H, Ar-H), 7.46 (d, *J* = 7.3 Hz, 2H, Ar-H), 7.37 – 7.20 (m, 5H, Ar-H), 7.08 – 7.04 (m, 1H, Ar-H), 6.94 – 6.88 (m, 4H, Ar-H), 6.85 – 6.82 (m, 1H, Ar-H), 5.68 (d, *J* = 4.6 Hz, 1H, 3’-OH), 5.34 (s, 1H, 1’-H), 4.32 (s, 1H, 2’-H), 4.29 (d, *J* = 4.6 Hz, 1H, 3’-H), 4.01 (d, *J* = 7.7 Hz, 1H, 5’-H), 3.88 (d, *J* = 7.7 Hz, 1H, 5’-H), 3.77 – 3.69 (m, 6H, Ar-OMe), 3.39 – 3.29 (m, 2H, 6’-CH_2).
^{13}C-NMR (126 MHz, DMSO) δ 158.1, 129.8, 129.5, 128.9, 127.7, 122.5, 113.2, 55.6, 55.0, 54.9.
TLC (Cy:EA 1:1) R_f = 0.67.
HRMS (MALDI) $[M+H]^+$ m/z = calculated: 629.26461, found: 629.26536.

β-anomer (**9**):

Yield: 0.138 mg (0.221 mmol, 92%).
^{1}H-NMR (500 MHz, DMSO) δ 8.02 (s, 1H, Ar-H), 7.80 (t, *J* = 7.5 Hz, 1H, Ar-H), 7.76 – 7.72 (m, 2H, Ar-H), 7.62 (dd, *J* = 16.1, 7.6 Hz, 2H, Ar-H), 7.55 (dt, *J* = 4.6, 2.5 Hz, 3H, Ar-H), 7.50 (d, *J* = 7.4 Hz, 2H, Ar-H), 7.38 – 7.25 (m, 3H, Ar-H), 7.21 (m, *J* = 16.9, 7.2, 5.8 Hz, 2H, Ar-H), 7.10 – 7.05 (m, 2H, Ar-H), 6.88 (m, *J* = 9.6, 7.0, 2.4 Hz, 2H, Ar-H), 6.86 – 6.82 (m, 2H, Ar-H), 5.42 (d, *J* = 4.7 Hz, 1H, 3‘-OH), 5.18 (s, 1H, 1‘-H), 4.25 (s, 1H, 2‘-H), 4.05 – 4.03 (m, 1H, 3‘-H), 3.94 (d, *J* = 7.2 Hz, 1H, 5‘-H), 3.85 (d, *J* = 7.4 Hz, 1H, 5‘-H), 3.70 (d, *J* = 4.9 Hz, 6H, Ar-OMe), 3.41 – 3.26 (m, 2H, 6‘-CH_2).
^{13}C-NMR (126 MHz, DMSO-*d*$_6$) δ 158.1, 157.8, 148.4, 140.3, 135.6, 129.8, 129.4, 128.9, 127.9, 127.7, 127.4, 126.5, 122.6, 113.2, 112.8, 85.8, 82.4, 79.9, 70.1, 59.8, 55.0, 54.9, 20.8.
TLC (Cy:EA 1:1) R_f = 0.63.
HRMS (MALDI) $[M+H]^+$ m/z = calculated: 629.26461, found: 629.26530.

(1*R*,3*S*,4*R*,7*S*)-7-[2-Cyanoethoxy(diisopropylamino)phosphinoxyl]-1-(4,4‘-dimethoxytrityloxymethyl)-1‘-(*m*-azobenzyl)-2,5-dioxabicyclo[2.2.1]heptane (**10**, **11**)

Compounds **8** (0.195 g, 0.310 mmol, 1.0 eq) or **9** (0.138 g, 0.221 mmol, 1.0 eq) were dissolved in 3 mL of dry DCM. DIPEA (0.200 g, 1.545 mmol, 5.0 eq / 0.143 g, 1.105 mmol, 5.0 eq) and CEO(N^{i}Pr$_2$)PCl (0.110 g, 0.465 mmol, 1.5 eq / 0.079 g, 0.332 mmol, 1.5 eq) were added successively and left to stir at room temperature for 2 h. Upon addition of methanol the reaction was evaporated to dryness, extracted with DCM, dried over Na_2SO_4 and evaporated to dryness again. The crude product was subjected to flash column chromatography (n-hexane:acetone 9:1 → 2:1) to afford the product as orange foam.

α-anomer (**10**):

Yield: 0.158 g (0.191 mmol, 51%).
^{1}H-NMR (500 MHz, DMSO-*d*$_6$) δ 8.01 (s, 1H, Ar-H), 7.93 – 7.89 (m, 2H, Ar-H), 7.87 – 7.83 (m, 1H, Ar-H), 7.66 – 7.58 (m, 4H, Ar-H), 7.48 – 7.44 (m, 2H, Ar-H), 7.35 – 7.29 (m, 4H, Ar-H), 7.27 – 7.22 (m, 2H, Ar-H), 6.93 – 6.87 (m, 5H, Ar-H), 6.87 – 6.83 (m, 1H, Ar-H), 5.43 (d, *J* = 4.4 Hz, 1H, 1’-H), 4.60 – 4.48 (m, 2H, 2’-H+3’-H), 4.05 (dd, *J* = 16.8, 7.9 Hz, 2H, CH_2+CH_2), 3.86 – 3.81 (m, 1H, CH_2), 3.79 – 3.71 (m, 7H, Ar-OMe+CH_2), 3.59 – 3.41 (m, 2H, CEO-CH_2), 2.67 – 2.60 (m, 2H, CH_2), 1.25 – 0.92 (m, 14H, ^{i}Pr).
^{13}C-NMR (126 MHz, DMSO-*d*$_6$) δ 158.1, 152.0, 151.8, 144.7, 137.7, 136.9, 136.6, 135.5, 134.9, 129.8, 129.7, 129.5, 127.9, 127.6, 126.7, 122.5, 113.2, 55.0, 24.3, 19.8, 19.8.
^{31}P-NMR (121 MHz, DMSO) δ 148.2, 148.1, 146.9, 146.8.
TLC (Cy:Aceton 2:1) R_f = 0.53.
HRMS (MALDI) $[M+H]^+$ m/z = calculated: 829.37246, found: 829.73083.

β-anomer (**11**):

Yield: 0.079 g (0.095 mmol, 43%)
1H-NMR (500 MHz, DMSO-*d*$_6$) δ 7.84 – 7.80 (m, 1H, Ar-H), 7.73 – 7.64 (m, 3H, Ar-H), 7.55 – 7.47 (m, 4H, Ar-H), 7.40 – 7.32 (m, 5H, Ar-H), 7.31 – 7.25 (m, 3H, Ar-H), 7.23 – 7.16 (m, 2H, Ar-H), 6.92 – 6.83 (m, 4H, Ar-H), 5.28 (d, *J* = 10.6 Hz, 1H, 1‘-H), 4.56 (s, 1H, 2‘-H), 4.39 (s, 1H, 3‘-H), 4.11 – 3.96 (m, 4H, CEO-CH_2+CH_2), 3.70 – 3.66 (m, 6H, Ar-OMe), 3.49 – 3.40 (m, 3H, 6‘-H+CH_2), 3.24 (d, 10.7 Hz, 1H, CH_2), 2.89 (t, *J* = 5.9 Hz, 2H, CEO-CH_2), 1.21 – 1.16 (m, 14H, iPr).
^{13}C-NMR (126 MHz, DMSO-*d*$_6$) δ 158.1, 152.2, 151.7, 141.1, 135.4, 129.8, 129.8, 129.7, 129.3, 129.3, 127.8, 127.8, 127.7, 126.7, 122.5, 118.6, 113.1, 113.1, 112.8, 112.3, 85.5, 82.6, 82.5, 58.2, 58.1, 54.9, 46.2, 44.5, 22.8, 22.7, 22.6, 22.6, 19.4, 19.3, 18.8.
^{31}P-NMR (121 MHz, DMSO-*d*$_6$) δ 147.6, 147.6, 147.2, 146.5.
TLC (Cy:Aceton 2:1) R_f = 0.53.
HRMS (MALDI) $[M]^+$ m/z = calculated: 828.36464, found: 828.92814.

2. Oligonucleotide synthesis

DNA synthesis

For the synthesis of DNA containing azobenzene-*C*-nucleosides, standard phosphoramidites were purchased from Sigma–Aldrich. The strands were synthesized in the 4,4′-dimethoxytrityl (DMTr)-On mode on an ABI392 synthesizer by using standard protocols and columns (1.0 µmol; Applied Biosystems). For the cleavage of nucleobase protection groups, a wash with diethylamine (25% in acetonitrile, 20 min.) followed by an acetonitrile wash and evaporation under reduced pressure were applied. Ammonia (25% in water) was used for resin-cleavage (over night, RT). After evaporation and resuspension in ultrapure water, the strands were purified by means of RP-HPLC with 0.4M hexafluoroisopropanol and 15 mM trimethylamine in ultrapure water and methanol (gradient: 5→40 % methanol over 40 min). Incubation with 80 % acetic acid for 20 min at room temperature cleaved the DMT-group. After evaporation, the strands were again purified by means of RP-HPLC as mentioned before. Mass-spectrometric analyses were recorded on a Bruker micrOTOF-Q device. The strands containing no azobenzene modifications were purchased from biomers.

RNA synthesis

For the synthesis of DNA containing azobenzene-*C*-nucleosides, standard phosphoramidites were purchased from Sigma–Aldrich. The strands were synthesized in the 4,4′-dimethoxytrityl (DMTr)-On mode on an ABI392 synthesizer by using standard protocols and columns (1.0 µmol; Applied Biosystems). For the cleavage of nucleobase protection groups, a wash with diethylamine (25% in acetonitrile, 20 min.) followed by an acetonitrile wash and evaporation under reduced pressure were applied. A 3:1 mixture of ammonia (25% in water) and ethanol was used for resin-cleavage (over night, RT). After evaporation the crude oligonucleotide was resuspended in 115 µL DMSO, 60 µL TEA and 75 µL TEA·3HF and incubated at 65 °C for 2.5 h. After cooling to room temperature 25 µL of aqueous sodium acetate (3 M) and 1mL of *n*-butanol was added and left at -80 °C. After precipitation the sample was centrifuged for 30 min. at 12.000 rpm and 4 °C, then supernatant was removed. The RNA-pellet was dried in a vacuum centrifuge, resuspended in ultrapure water and purified by means of RP-HPLC with 0.4M hexafluoroisopropanol and 15 mM trimethylamine in ultrapure water and methanol (gradient: 5→40 % methanol over 40 min). Incubation with 80 % acetic acid for 20 min at room temperature cleaved the DMT-group. After evaporation, the strands were again purified by means of RP-HPLC as mentioned before. Mass-spectrometric analyses were recorded on a Bruker micrOTOF-Q device. The strands containing no azobenzene modifications were purchased from biomers.

Oligonucleotide sequences and masses

Oligo	Name	Sequence 5'→3'	X =	$M_{calculated}$ [g·mol^{-1}]	M_{found} [g·mol^{-1}]
DNA	Strand 1	FAM-GTG-GCA-AGG-T		3646	3645
DNA	Strand 2	FAM-GTG-GXA-AGG-T	abasic site	3535	3536
RNA	Strand 3	FAM-GUG-GCA-AGG-U		3777	3779
DNA	Strand 4	ACC-TTG-CCA-C-DAB		3408	3409
DNA	Strand 5	ACC-TTX-CCA-C-DAB	DNAzo	3439	3440
DNA	Strand 6	ACC-TTX-CCA-C-DAB	LNAzo α	3467	3468
DNA	Strand 7	ACC-TTX-CCA-C-DAB	LNAzo β	3467	3468
RNA	Strand 8	ACC-UUG-CCA-C-DAB		3541	3541
RNA	Strand 9	ACC-UUX-CCA-C-DAB	DNAzo	3556	3559
RNA	Strand 10	ACC-UUX-CCA-C-DAB	LNAzo α	3584	3587
RNA	Strand 11	ACC-UUX-CCA-C-DAB	LNAzo β	3584	3587
DNA	Strand 12	ACC-TTG-CCA-C		2948	2939
DNA	Strand 13	GTG-GCA-AGG-T		3108	3100
DNA	Strand 14	ACC-TXG-CCA-C	abasic site	2823	2827
DNA	Strand 15	ACC-TTX-CCA-C	abasic site	2798	2804
DNA	Strand 16	GTG-GXA-AGG-T	abasic site	2998	2999
DNA	Strand 17	GTG-GCX-AGG-T	abasic site	2974	2968

System 1: Strand 1 + 4/5/6/7
System 2: Strand 2 + 4/5/6/7
System 3: Strand 3 + 4/5/6/7
System 4: Strand 3 + 8/9/10/11

3. Spectroscopic studies

3.1 Spectra of pure LNAzo β

For spectra of free nucleoside **7**, three independent samples with a concentration of 36 µM, 63 µM and 90 µM in a solution of water and acetonitrile (95:5) were separated on a short precolumn under isocratic conditions. The spectra of baseline separated peaks from both photoisomers were superimposed to find an isosbestic point at 378 nm. From the three concentrations, the extinction coefficients at the isosbestic point could be calculated to normalize spectra of the pure compounds (to be seen in Figure S2).

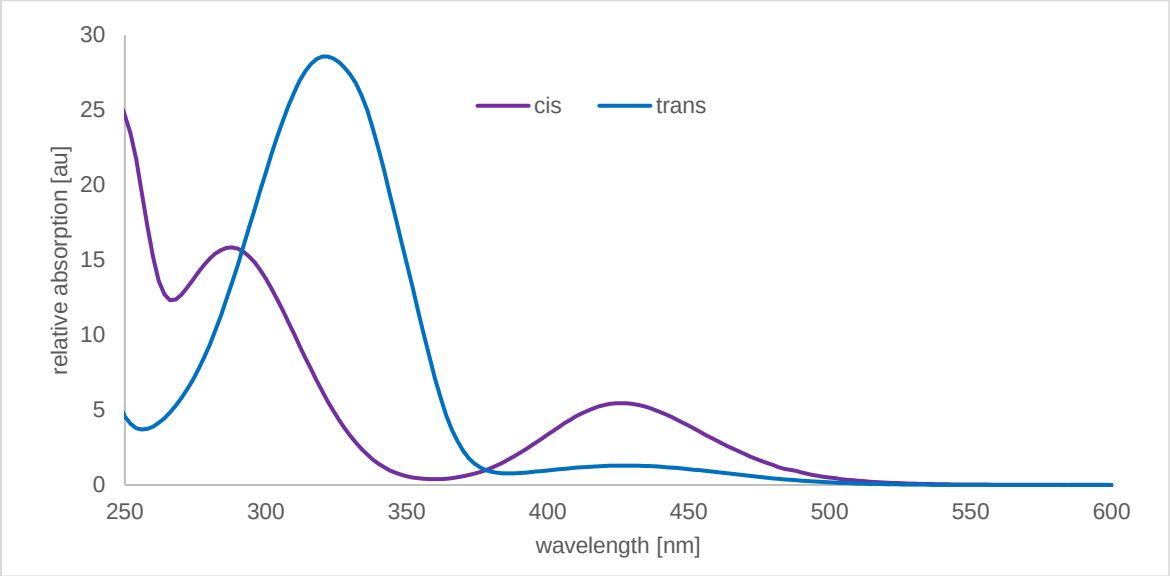

Figure S2: normalized spectra of the cis and trans photoisomers of nucleoside 7.

3.2 Photostationary distributions of LNAzo β

Three independent samples of compound **7** (100 nmol) were irradiated either at 365 nm or 420 nm until the photostationary state was reached (365 nm: 220 mW, 60 s; 420 nm: 290 mW, 30 s). Photoisomers were then baseline-separated on a short precolumn by means of RP-HPLC under isocratic conditions (95% 0.4 M trimethylammonium acetate buffer pH 7, 5% ACN) and spectra were recorded with an inline diode array detector. A chromatogram trace at the isosbestic point (378 nm) was extracted (Figure S3a). From the integrals of the peaks, the relative amount of the photoisomers was determined. Under these conditions, the photostationary state was determined to be at 80.0±0.5% cis isomer after irradiation at 365 nm and at 20.3±0.1% cis isomer after irradiation at 420 nm.

Alternatively, the photostationary distribution can be calculated from absorbance ratios of the n-π*-band at 420 nm. This analysis showed that the photostationary state after irradiation at 365 nm was composed of 79±1% cis isomer and the photostationary state after irradiation at 420 nm of 21±1% cis isomer, respectively.

Details of this analysis can be seen in Figure S3.

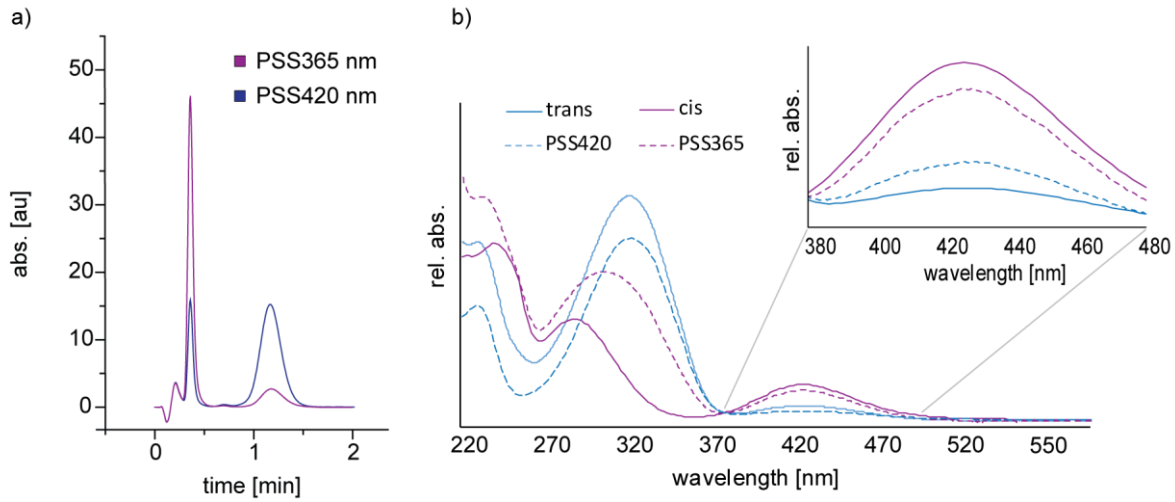

Figure S3: Analysis of the photostationary distribution of the photostationary states at 365 nm and 420 nm with either RP-HPLC (a) or the absorption spectra of the photostationary states in comparison to the absorption spectra of the pure photoisomers.

3.3 Photofatigue studies of LNAzo β

For evaluation of the photofatigue resistance of 7, a 100 µM sample in 1x PBS was alternately irradiated with 365 nm (220 mW, 60 s) and 420 nm (290 mW, 30 s) and absorption changes at 300 nm were recorded. Compound 7 showed no photofatigue over 100 switching cycles (see Figure S4).

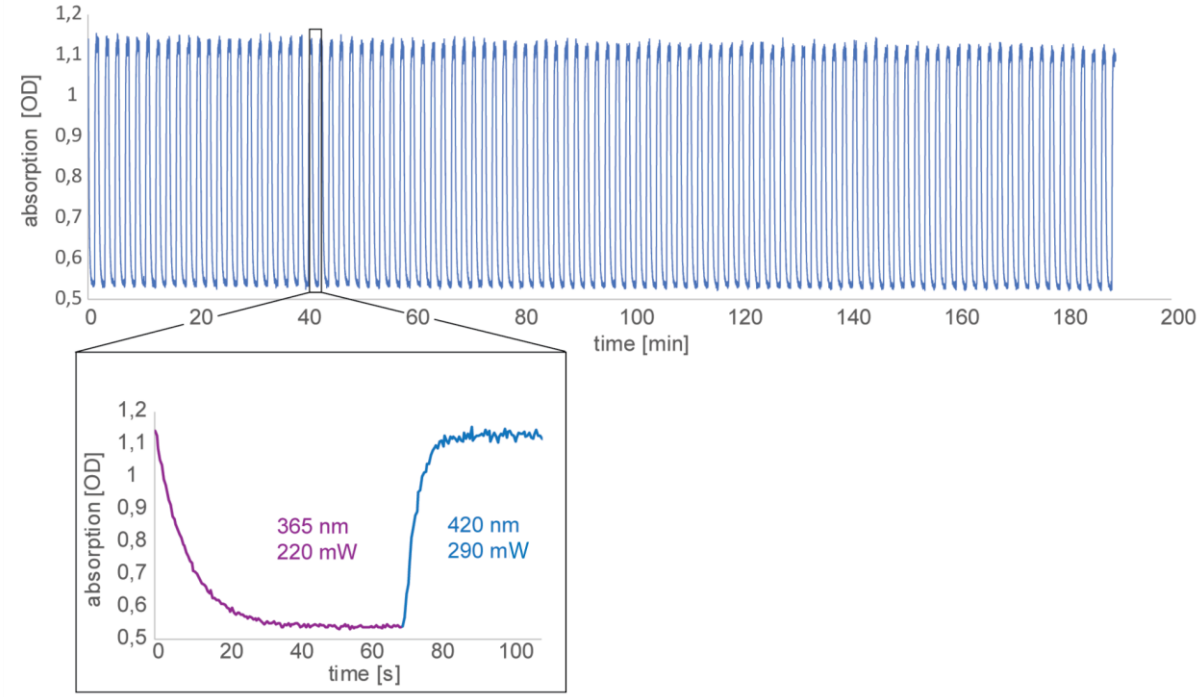

Figure S4: display of 100 switching cycles of 7 with a close-up of one cycle.

4. Melting temperature studies

For melting temperature measurements 1 mL samples were prepared with 1µM of strand and counterstrand in 1x PBS-buffer for each modification and each system (16 in total). The absorbance changes at 260 nm were measured by a V-650 UV/vis-spectrometer from JASCO. Samples were irradiated as single strands at elevated temperatures (system 1-3: 70°C, system 4: 80°C) with either 365 nm or 420 nm until the photostationary state (PSS) was reached to prevent mismatches. The Temperature gradient was 1 °C per min. To avoid effects of hysteresis, melting temperatures were calculated by a sigmoidal fit from cooling and heating measurements. At least five independent heating and cooling measurements were performed for precise results. For experimental values with error bars see Figures S5-8. The melting curves shown in 4.2 show the cooling (1-5) and heating (1r-5r) of the duplexes.

4.1 Summary of the melting temperatures

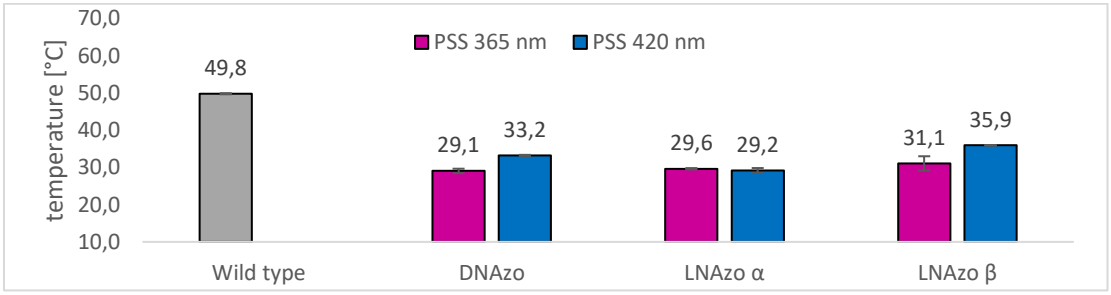

Figure S5: Melting temperatures of system 1.

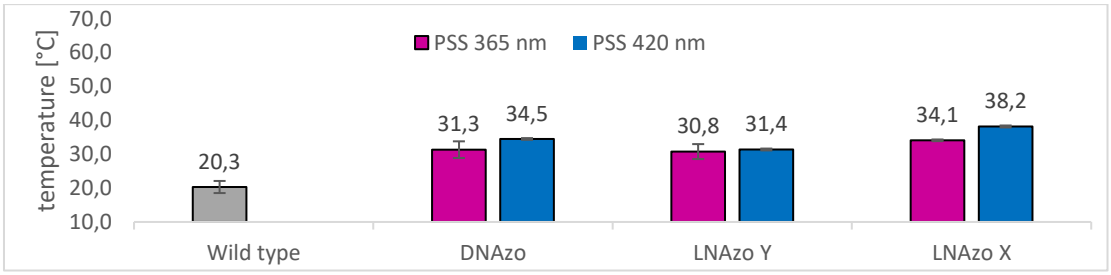

Figure S6: Melting temperatures of system 2.

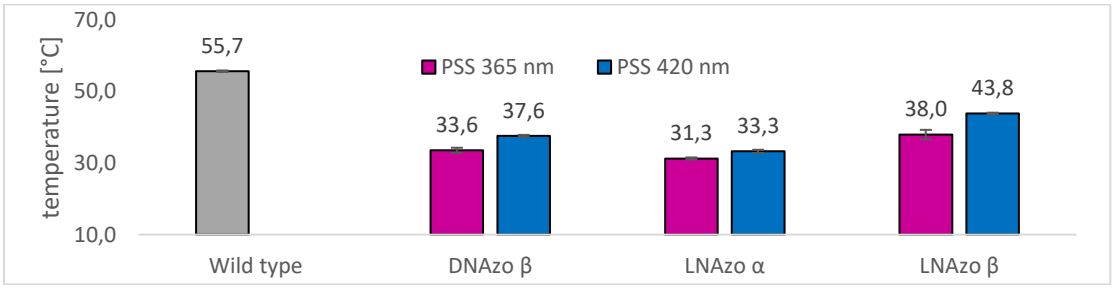

Figure S7: Melting temperatures of system 3.

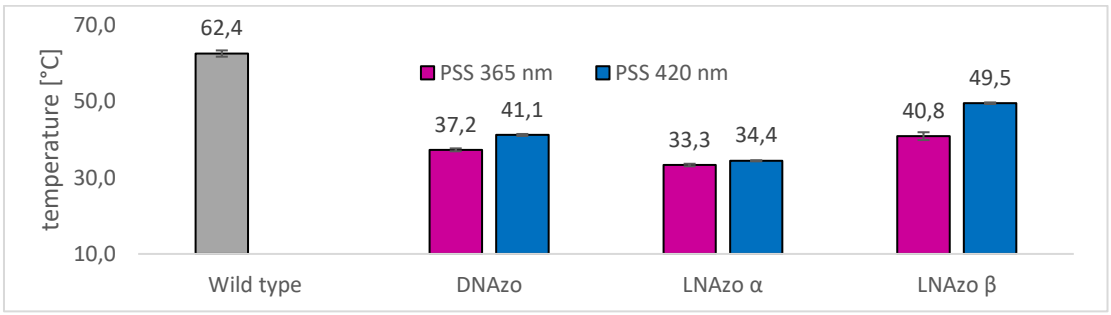

Figure S8: Melting temperatures of system 4.

4.2 Melting curves of the duplexes

4.2.1 System 1

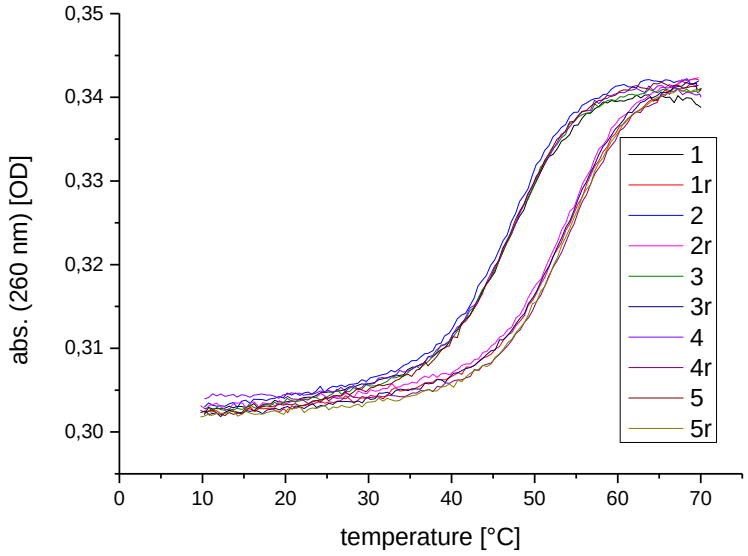

Figure S8: Melting curves of system 1 wild type.

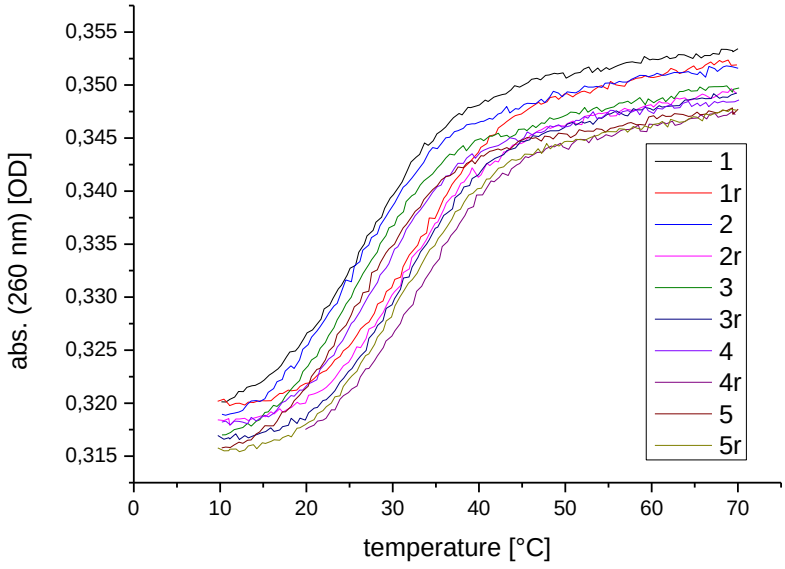

Figure S9: Melting curves of system 1 DNAzo PSS365 nm.

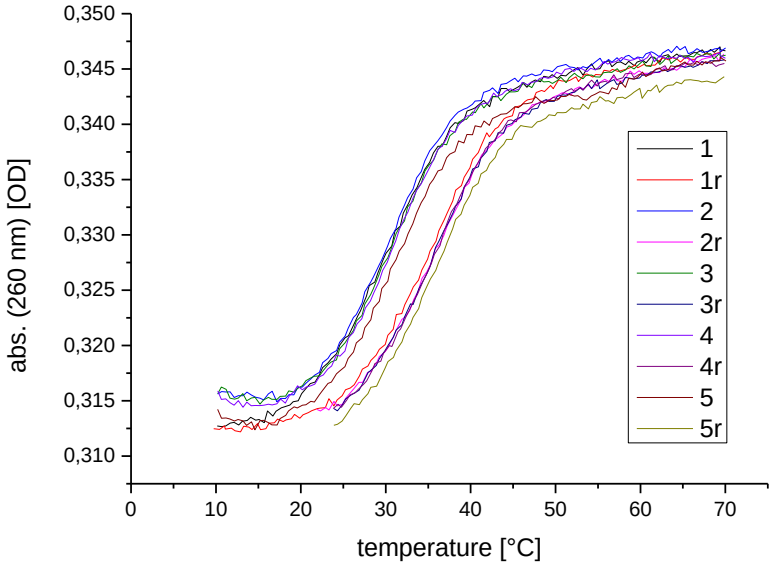

Figure S10: Melting curves of system 1 DNAzo PSS420 nm.

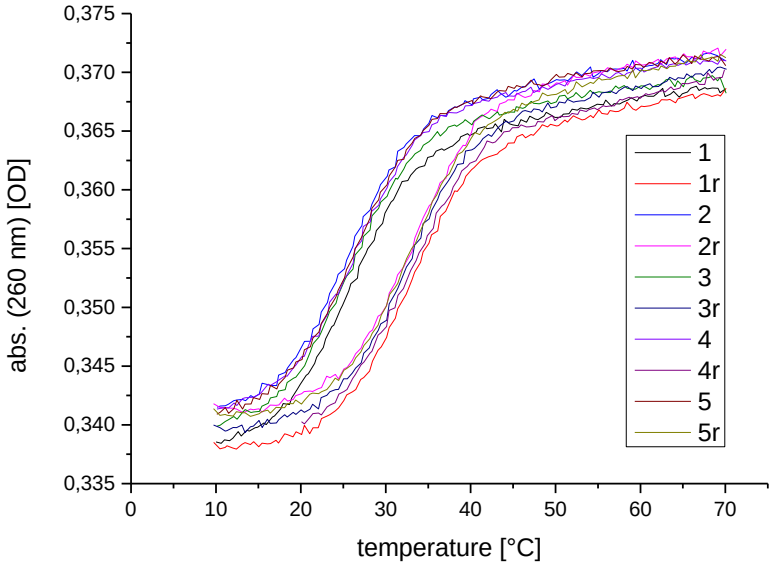

Figure S10: Melting curves of system 1 LNAzo α PSS365 nm.

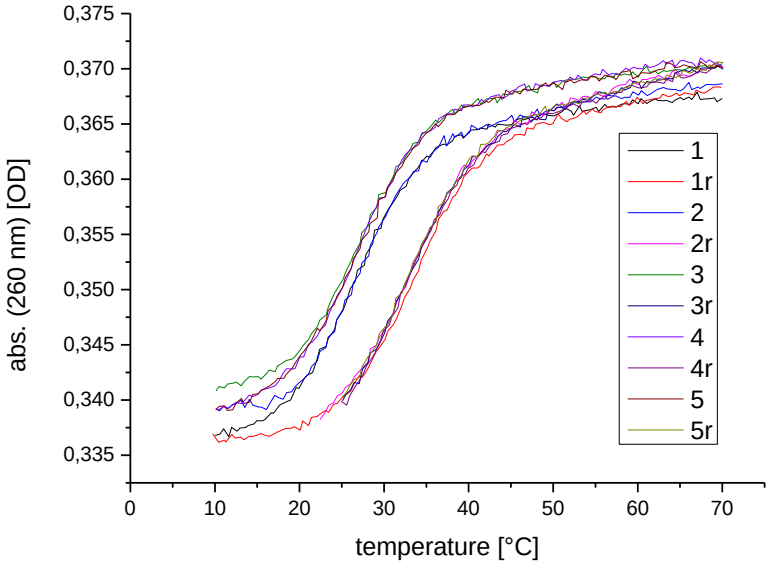

Figure S11: Melting curves of system 1 LNAzo α PSS420 nm.

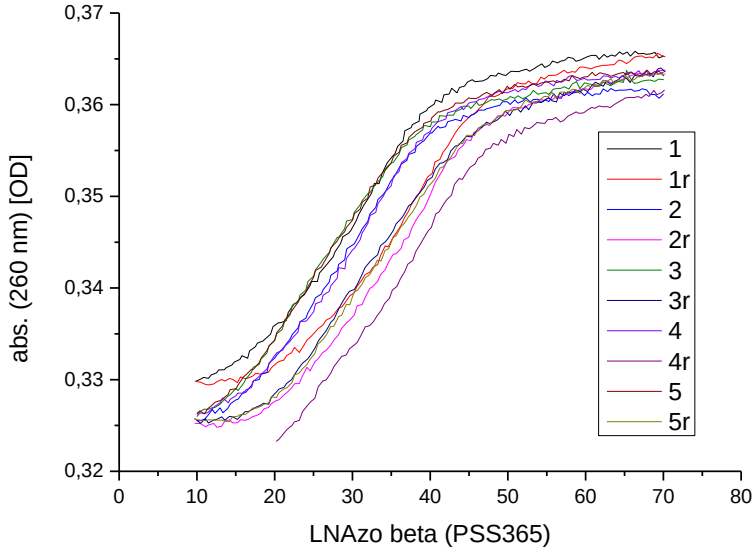

Figure S12: Melting curves of system 1 LNAzo β PSS365 nm.

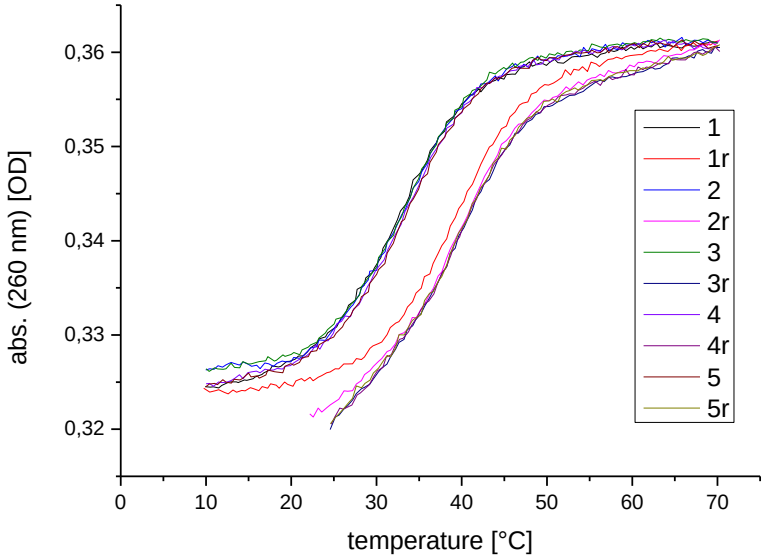

Figure S13: Melting curves of system 1 LNAzo β PSS420 nm.

4.2.2 System 2

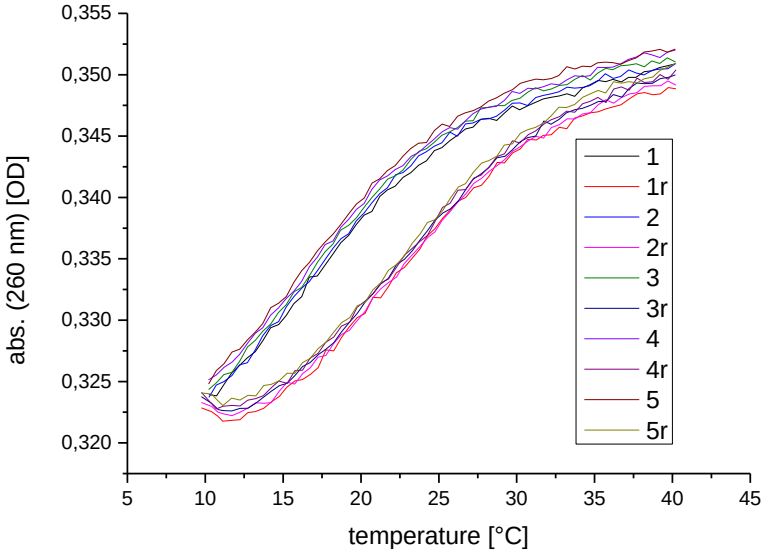

Figure S14: Melting curves of system 2 wild type.

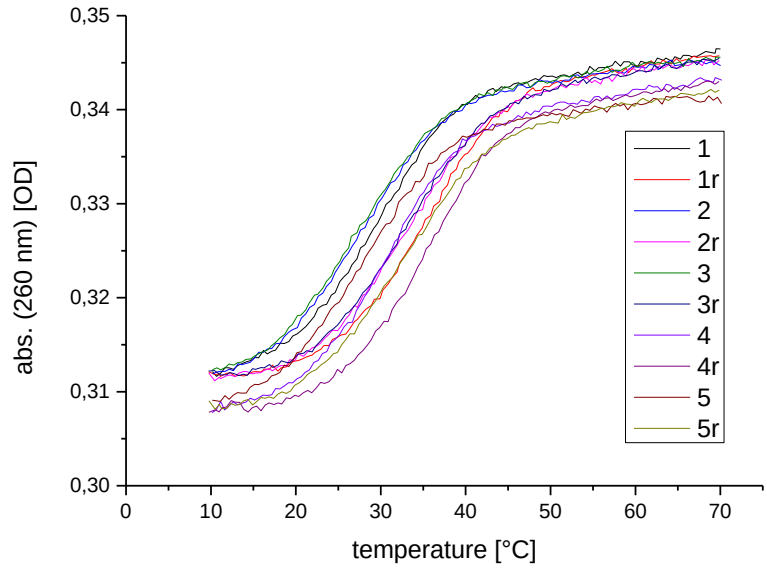

Figure S15: Melting curves of system 2 DNAzo PSS365 nm.

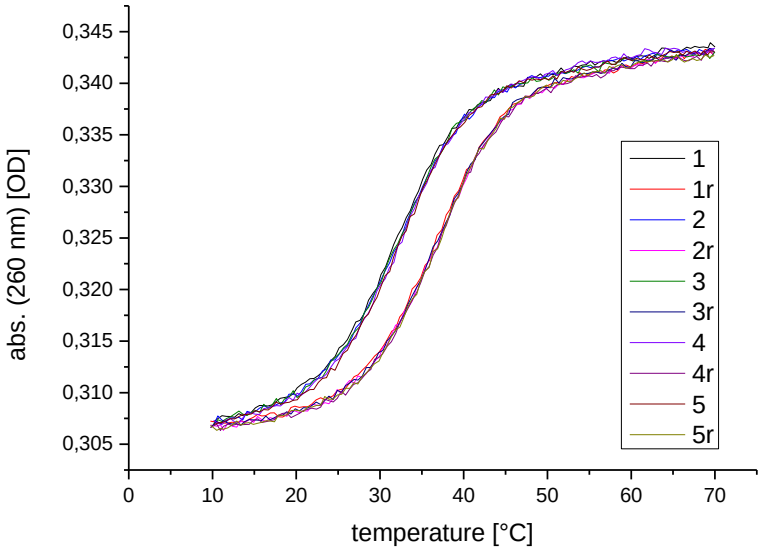

Figure S16: Melting curves of system 2 DNAzo PSS420 nm.

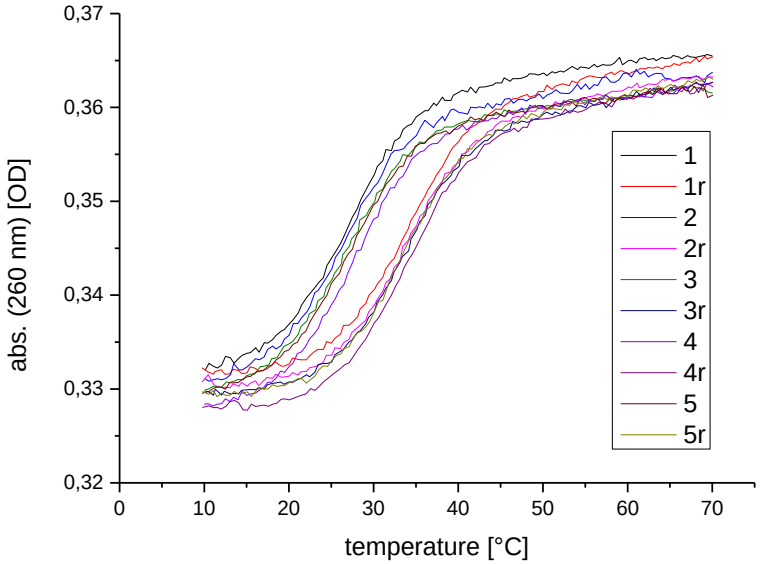

Figure S17: Melting curves of system 2 LNAzo α PSS365 nm.

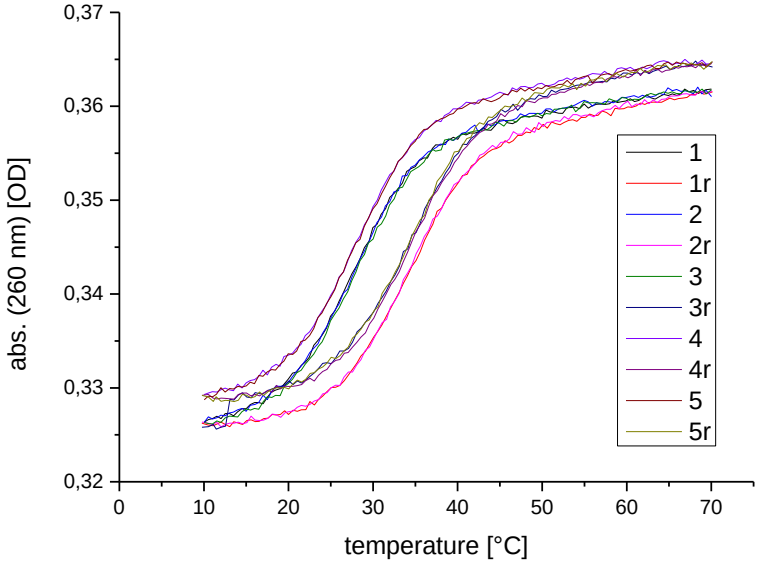

Figure S18: Melting curves of system 2 LNAzo α PSS420 nm.

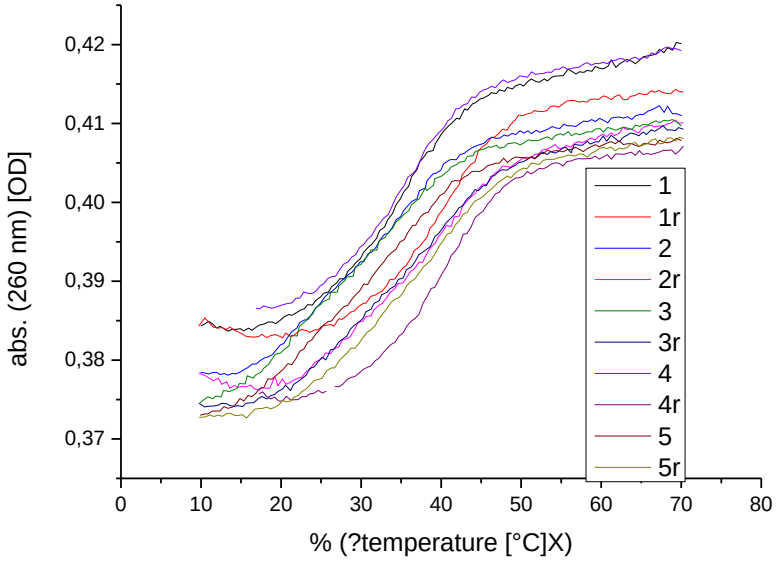

Figure S19: Melting curves of system 2 LNAzo β PSS365 nm.

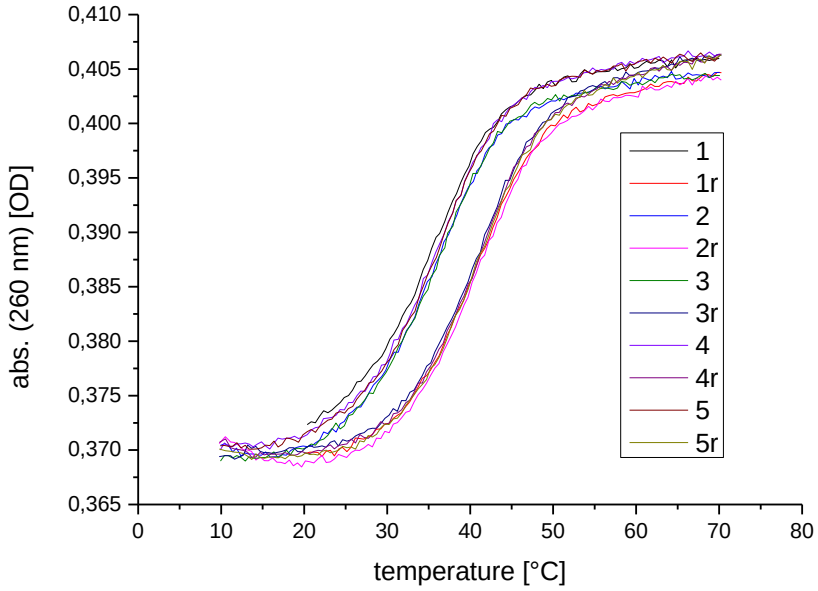

Figure S20: Melting curves of system 2 LNAzo β PSS420 nm.

4.2.3 System 3

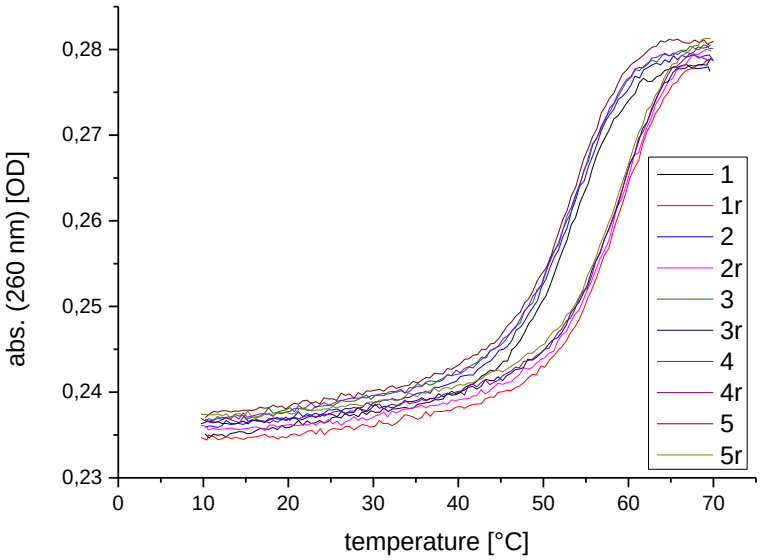

Figure S21: Melting curves of system 3 wild type.

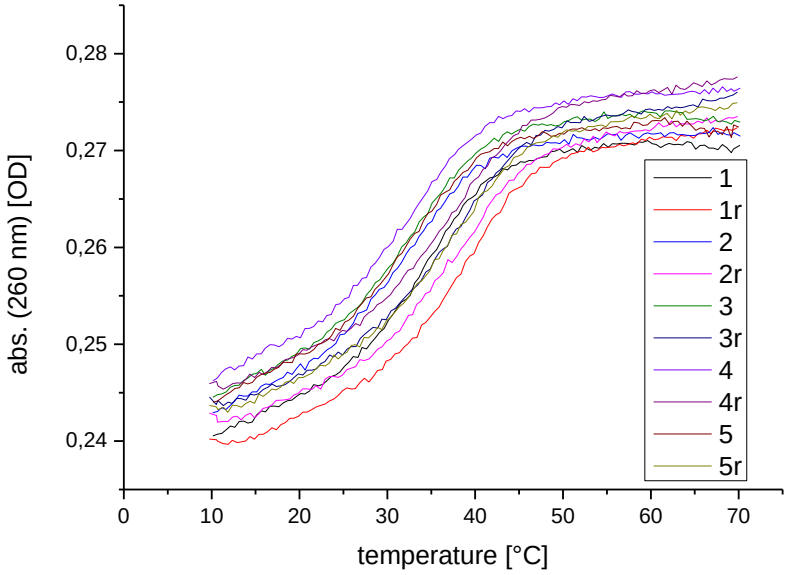

Figure S22: Melting curves of system 3 DNAzo PSS365 nm.

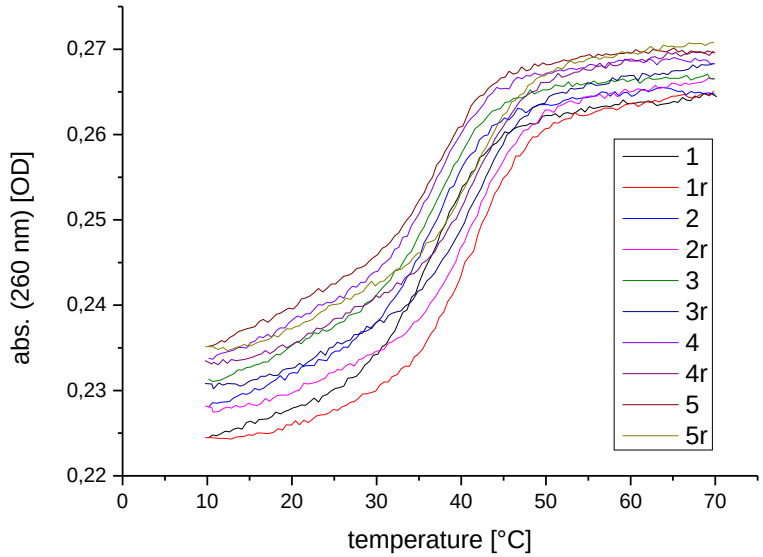

Figure S23: Melting curves of system 3 DNAzo PSS420 nm.

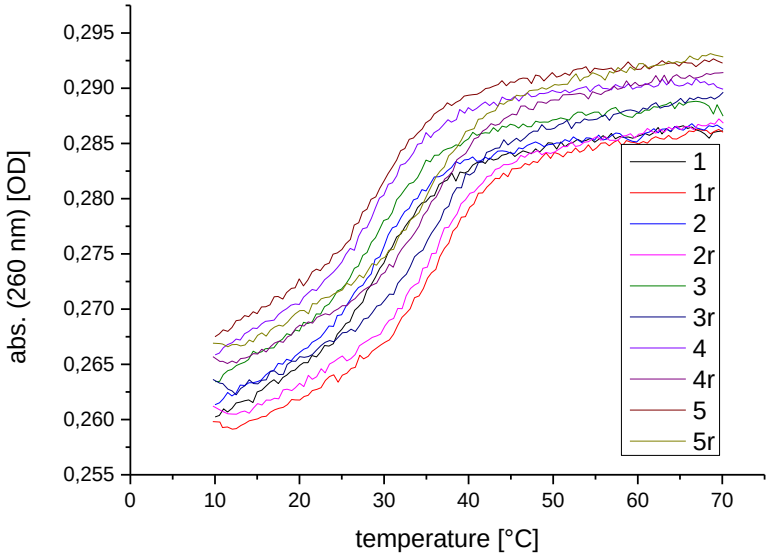

Figure S24: Melting curves of system 3 LNAzo α PSS365 nm.

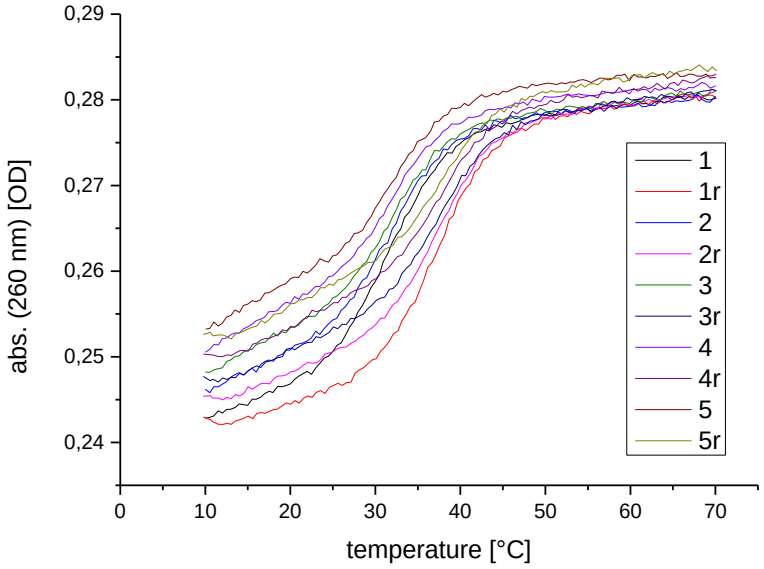

Figure S25: Melting curves of system 3 LNAzo α PSS420 nm.

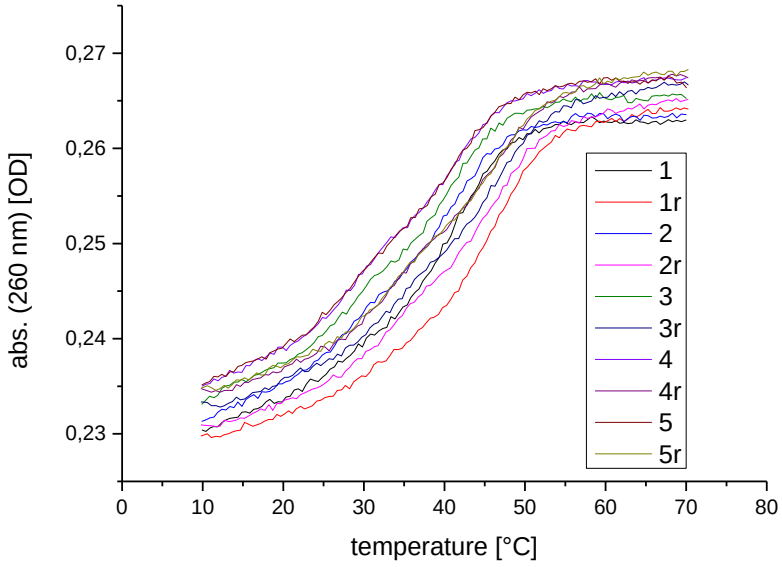

Figure S26: Melting curves of system 3 LNAzo β PSS365 nm.

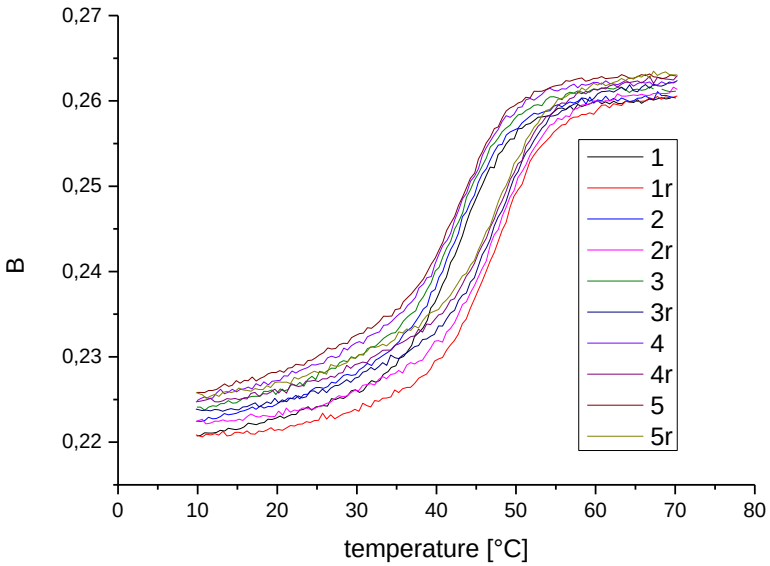

Figure S27: Melting curves of system 3 LNAzo β PSS420 nm.

4.2.4 System 4

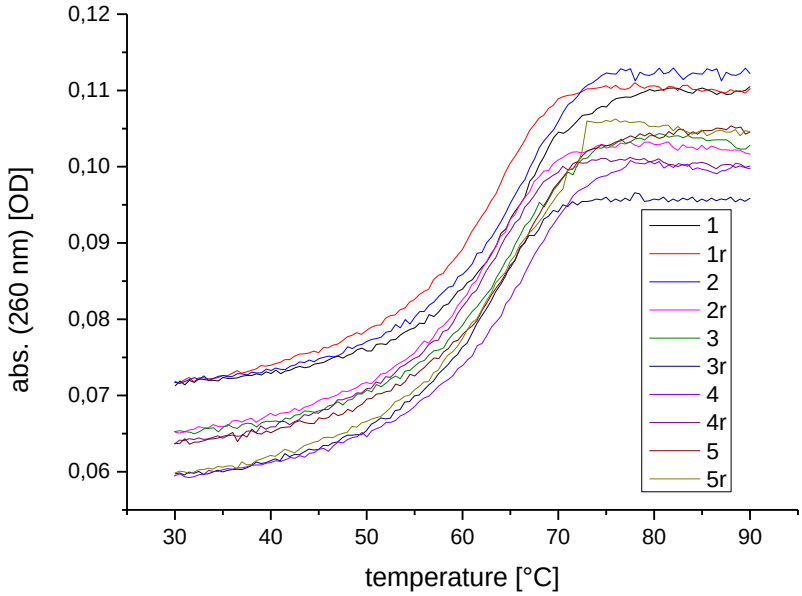

Figure S28: Melting curves of system 4 wild type.

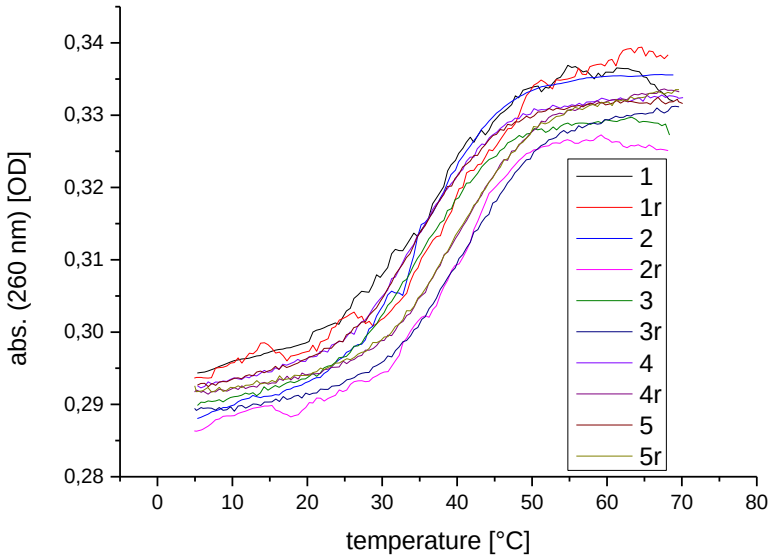

Figure S29: Melting curves of system 4 DNAzo PSS365 nm.

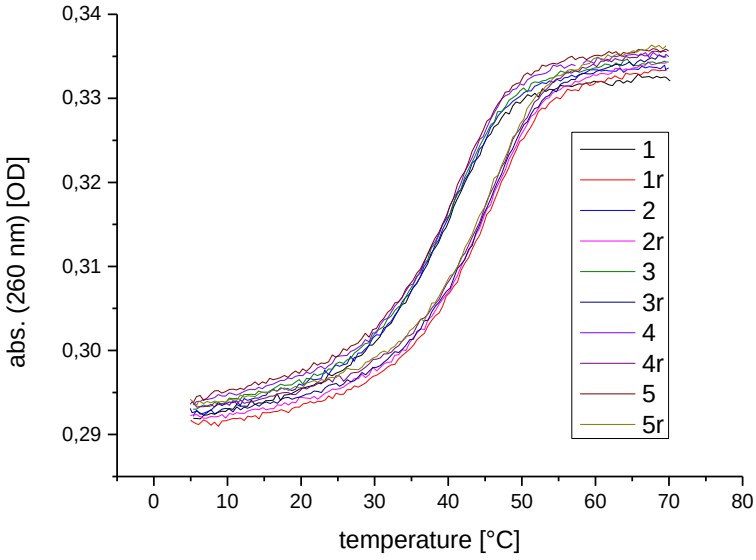

Figure S30: Melting curves of system 4 DNAzo PSS420 nm.

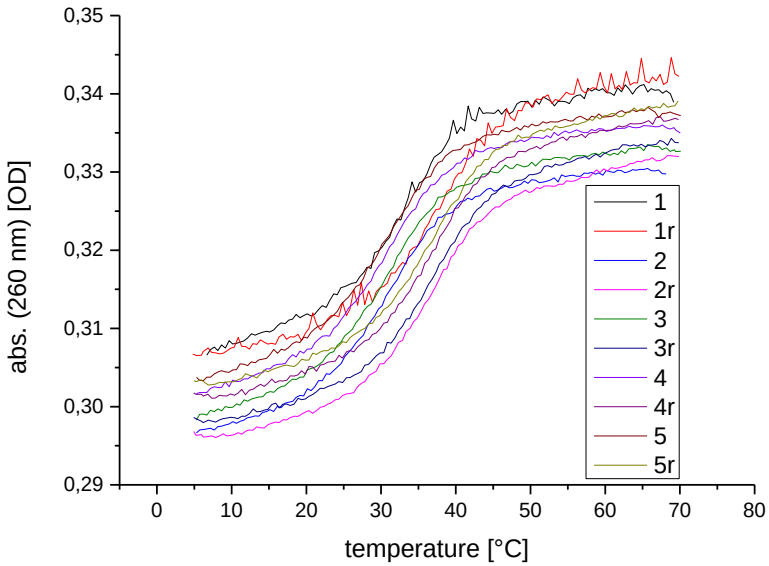

Figure S31: Melting curves of system 4 LNAzo α PSS365 nm.

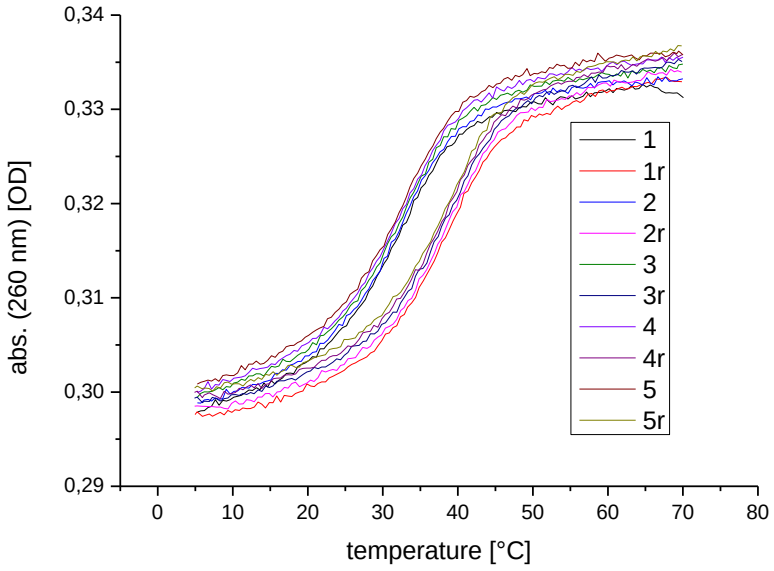

Figure S32: Melting curves of system 4 LNAzo α PSS420 nm.

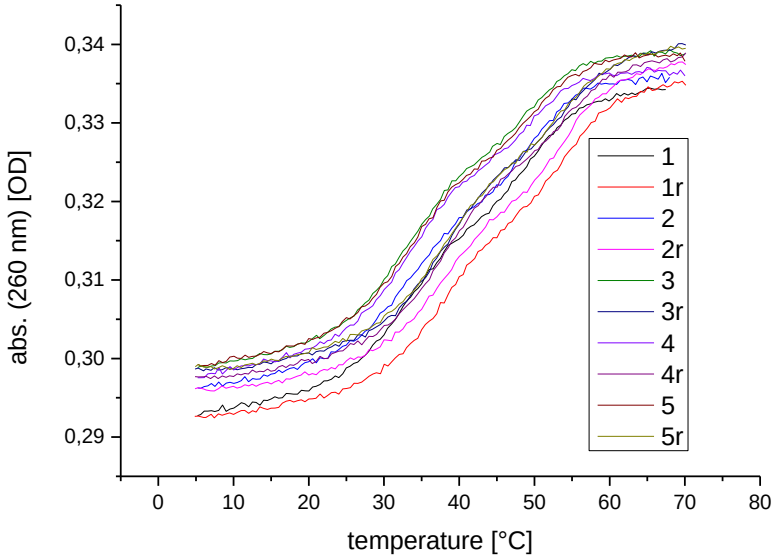

Figure S33: Melting curves of system 4 LNAzo β PSS365 nm.

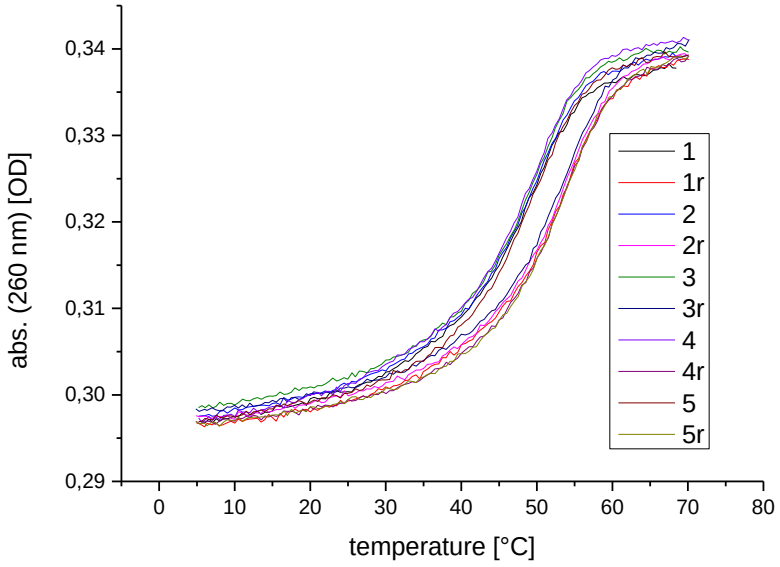

Figure S34: Melting curves of system 4 LNAzo β PSS420 nm.

5. CD-specroscopic studies

Samples for CD-measurements had a concentration of 10 µM in 1x PBS-buffer. CD-spectra were recorded on a J-710 CD-spectrometer from *JASCO*. Samples were irradiated at 70 °C, then cooled and measured at 20 °C. Ten individual measurements were accumulated for each spectrum for best results.

5.1 System 1

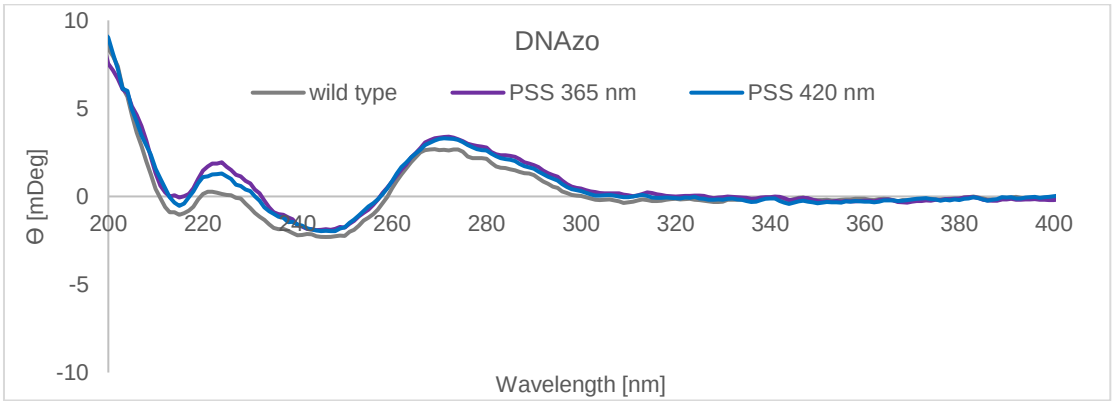

Figure S35: CD-spectra of strand 1+5 compared to strand 1+4.

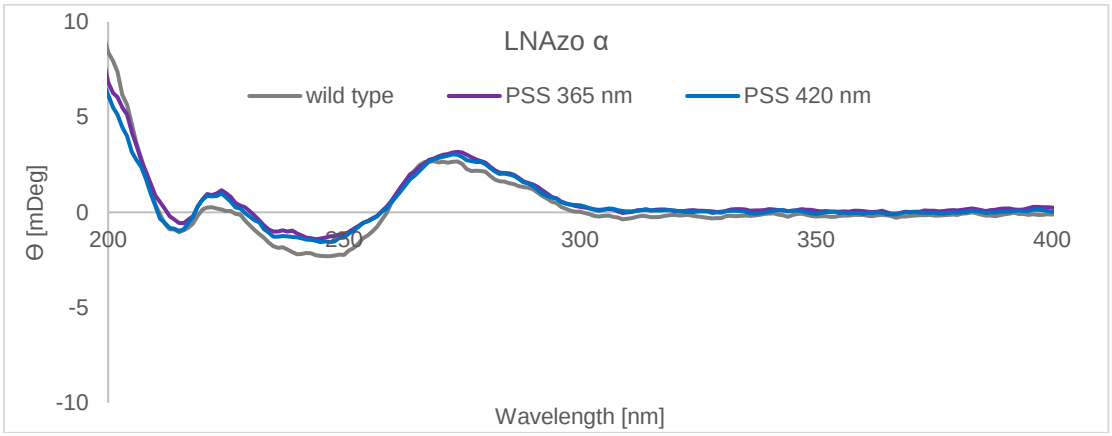

Figure S36: CD-spectra of strand 1+6 compared to strand 1+4.

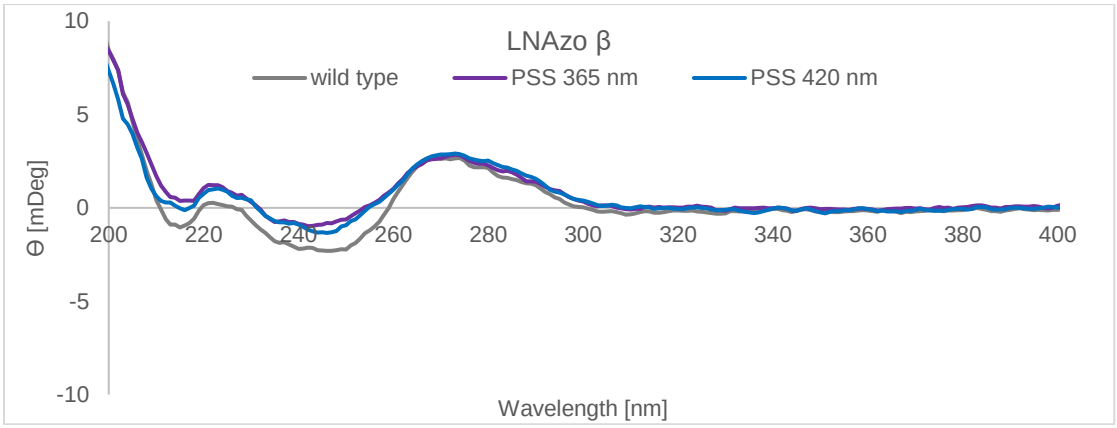

Figure S37: CD-spectra of strand 1+7 compared to strand 1+4.

5.2 System 2

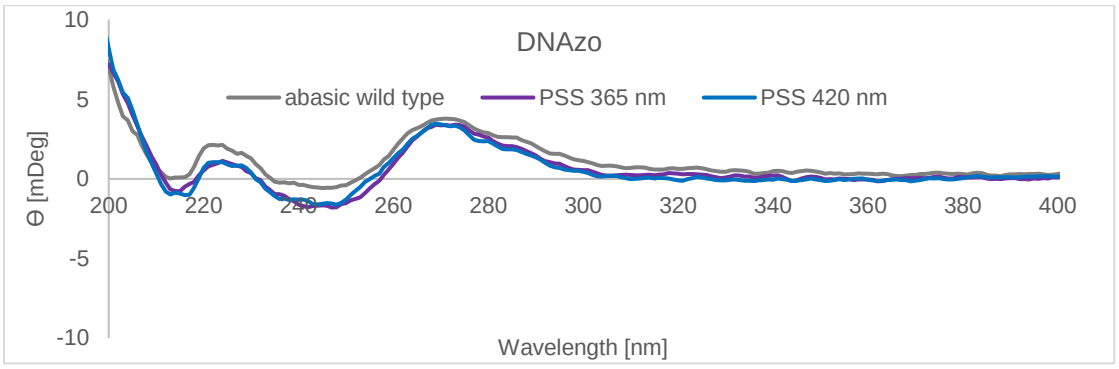

Figure S38: CD-spectra of strand 2+5 compared to strand 2+4.

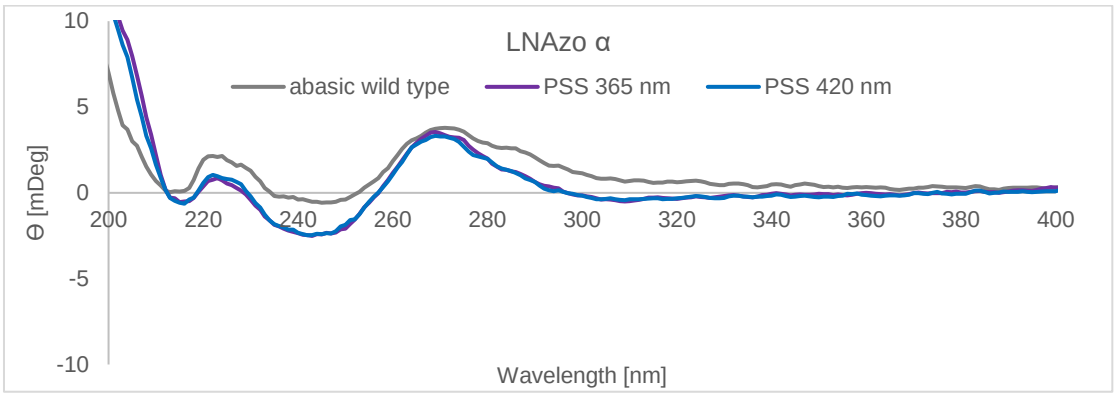

Figure S39: CD-spectra of strand 2+6 compared to strand 2+4.

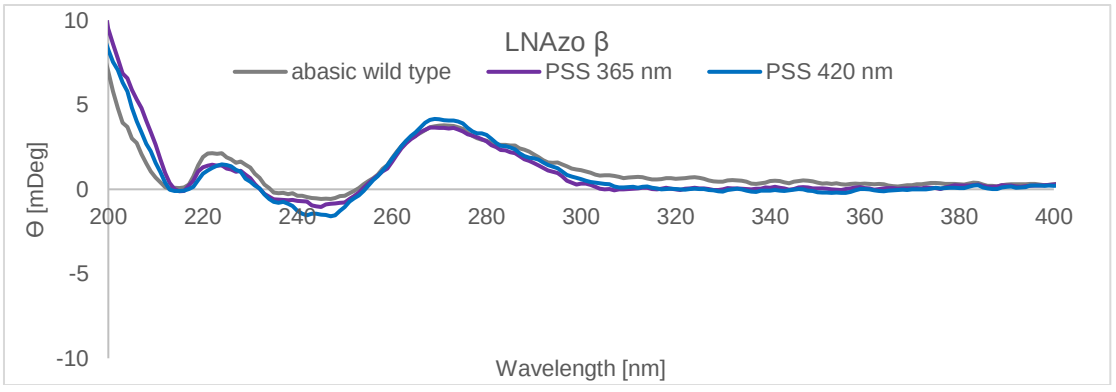

Figure S40: CD-spectra of strand 2+7 compared to strand 2+4.

5.3 System 3

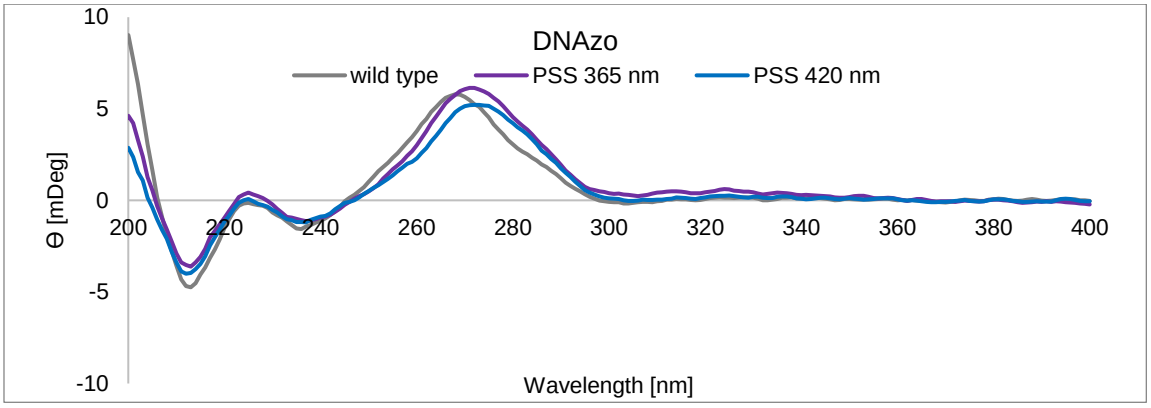

Figure S41: CD-spectra of strand 3+5 compared to strand 3+4.

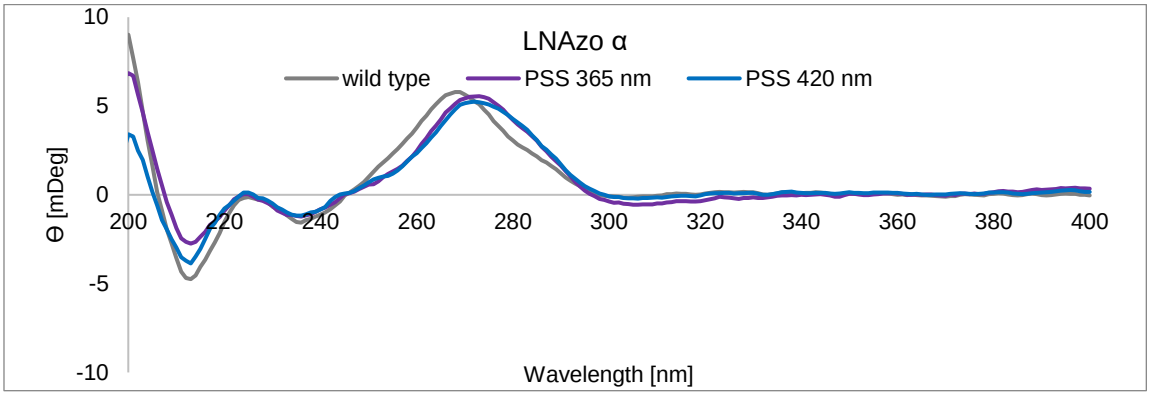

Figure S42: CD-spectra of strand 3+6 compared to strand 3+4.

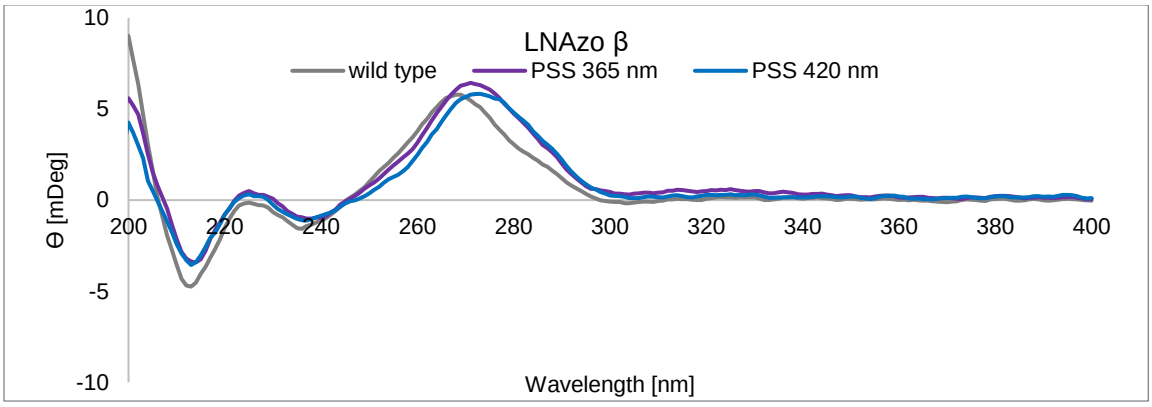

Figure S43: CD-spectra of strand 3+7 compared to strand 3+4.

5.3 System 4

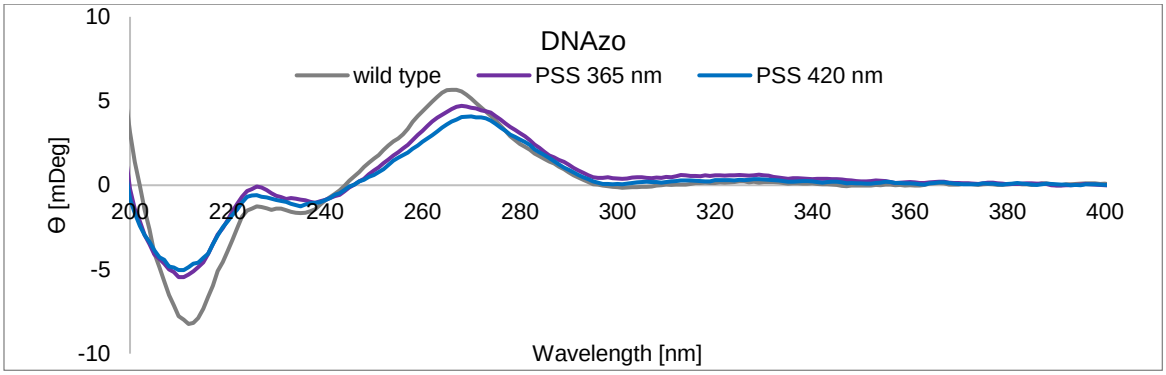

Figure S44: CD-spectra of strand 3+9 compared to strand 3+8.

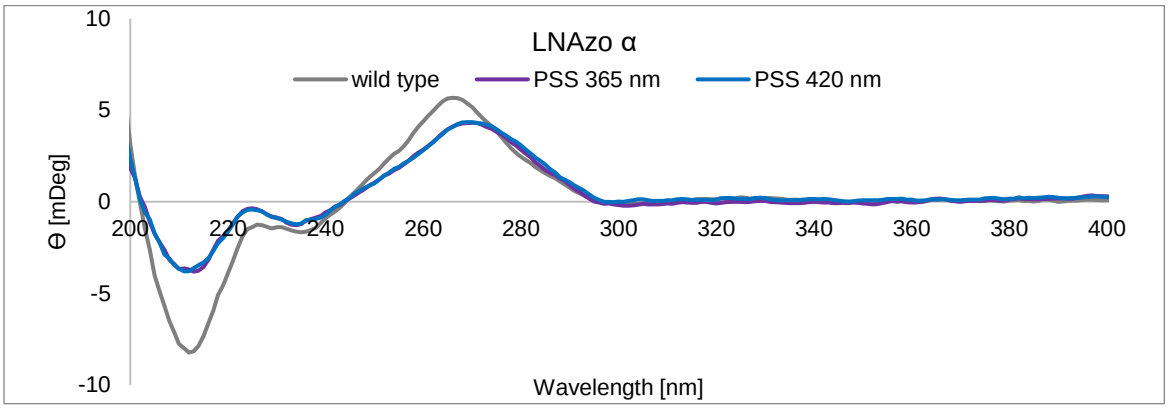

Figure S45: CD-spectra of strand 3+10 compared to strand 3+8.

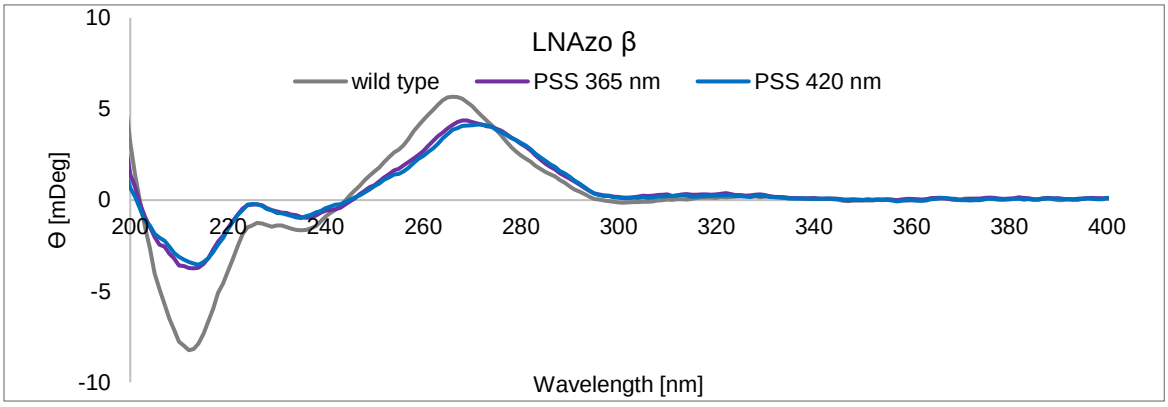

Figure S46: CD-spectra of strand 3+11 compared to strand 3+8.

6. Fluorescence-based studies

Temperature-dependent fluorescence measurements were recorded in a PikoReal real-time PCR system from *Thermo Scientific.* Triplicates were irradiated at 80 °C, then temperature dependent fluorescence was measured from 80 °C to 5 °C within 1 h. Values given are averaged over these three individual samples. Measured spectra were normalized with the spectra of free fluorescein in PBS buffer of the corresponding concentration to level out temperature-dependence of fluorescein fluorescence followed by sigmoidal fit with Origin. The inflection points of resulting fits are given as melting temperatures. Melting temperatures are given as column graphs in Figure S20-34, corresponding melting temperatures in [°C] above the graphs, concentrations in [µmol/L] below the graphs starting on the following page. The corresponding wild type was included as a negative control, as irradiation at different wavelength should not alter melting temperatures. In some cases, sigmoidal fit to curves with abnormal course could not be executed, indicated by missing columns.

6.1 System 1

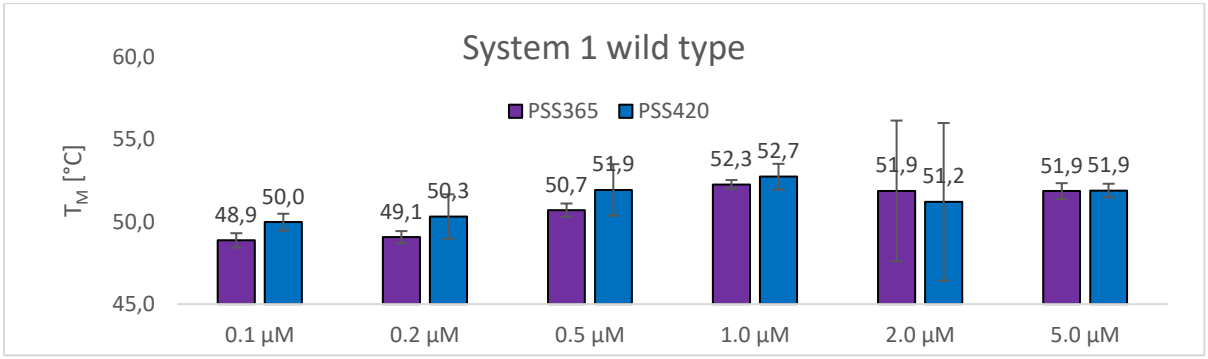

Figure S47: Bar graph of fluorescence-based melting temperatures of system 1 wild type.

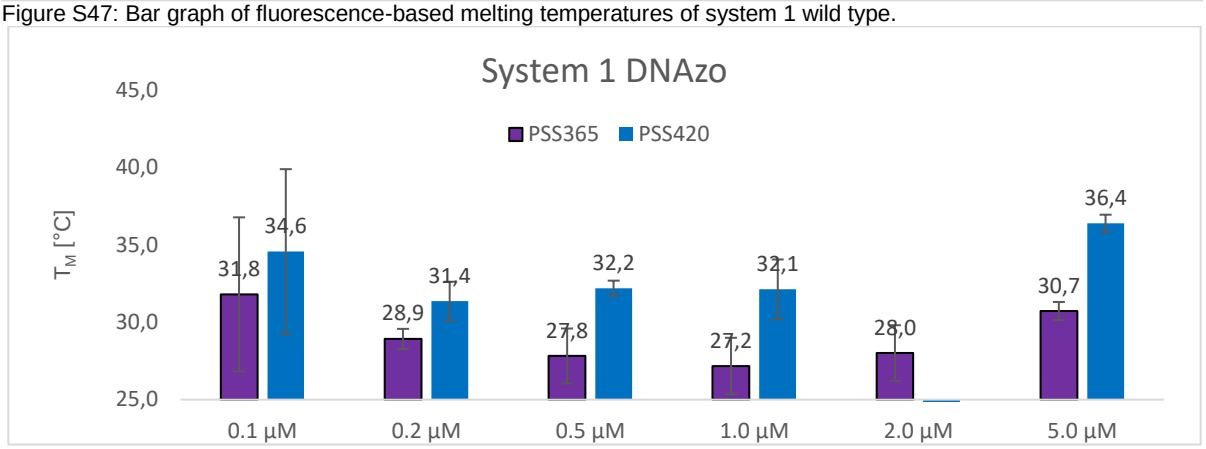

Figure S48: Bar graph of fluorescence-based melting temperatures of system 1 DNAzo.

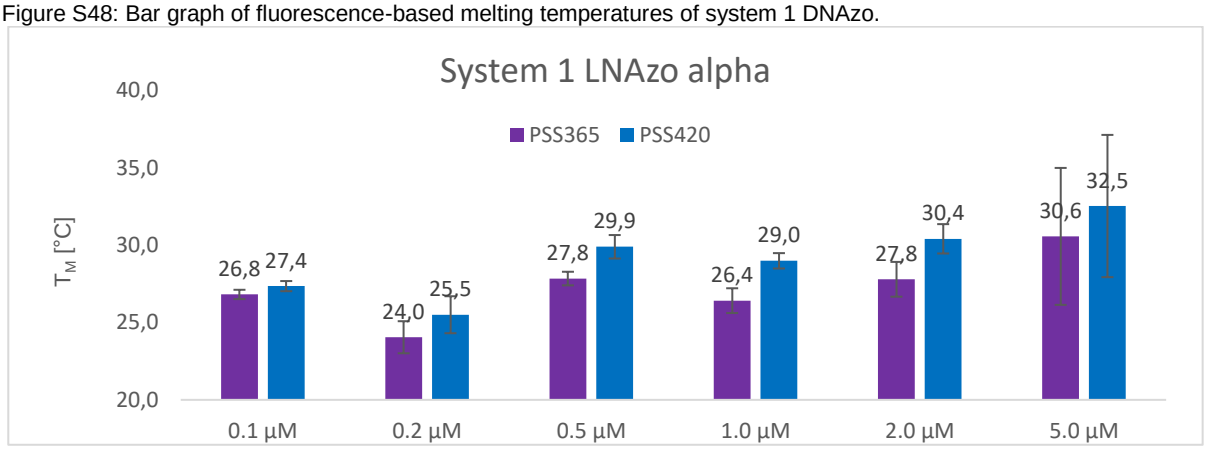

Figure S49: Bar graph of fluorescence-based melting temperatures of system 1 LNAzo α.

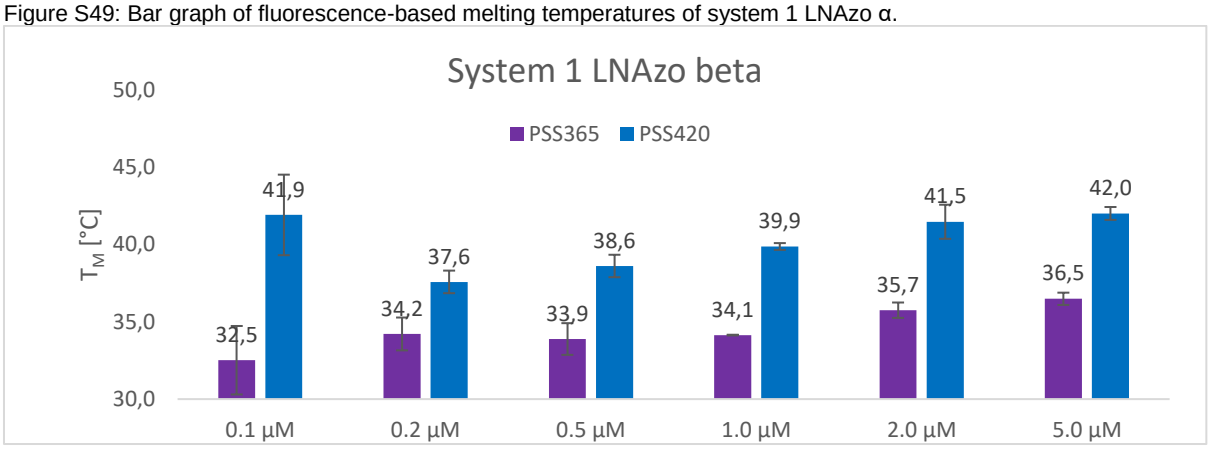

Figure S50: Bar graph of fluorescence-based melting temperatures of system 1 LNAzo β.

6.2 System 2

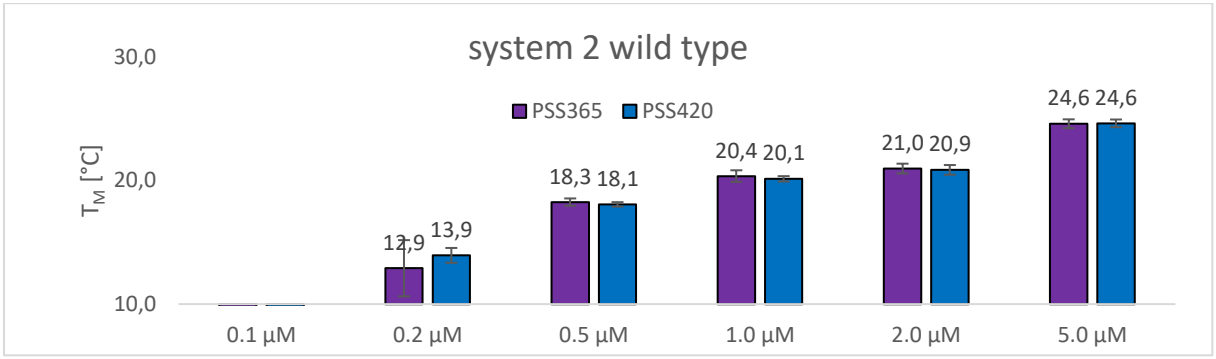

Figure S51: Bar graph of fluorescence-based melting temperatures of system 2 wild type.

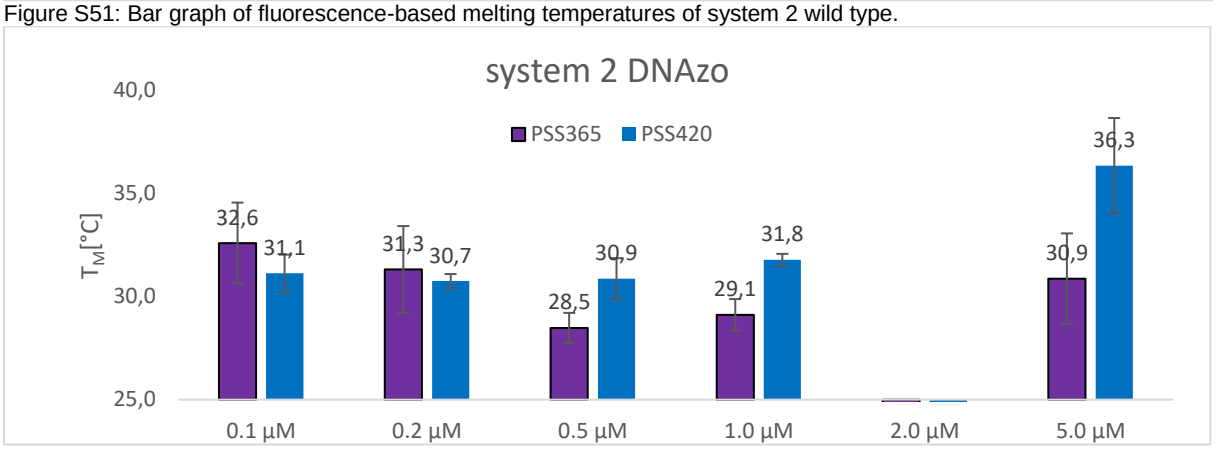

Figure S52: Bar graph of fluorescence-based melting temperatures of system 2 DNAzo.

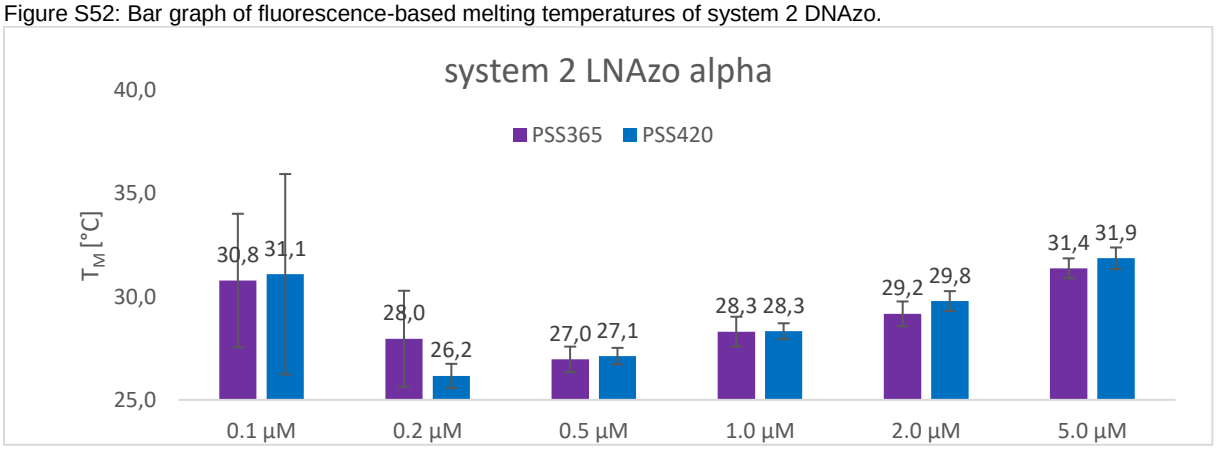

Figure S53: Bar graph of fluorescence-based melting temperatures of system 2 LNAzo α.

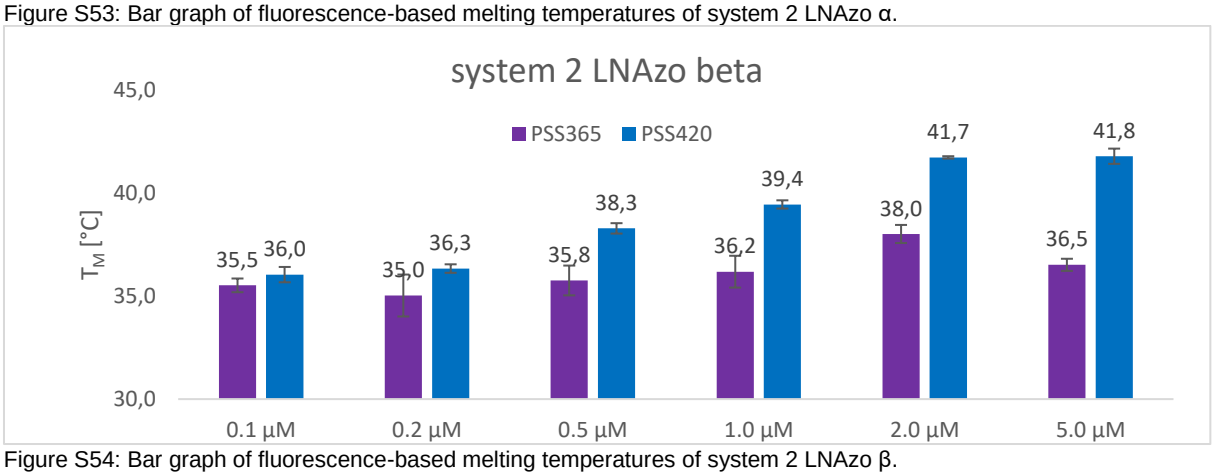

Figure S54: Bar graph of fluorescence-based melting temperatures of system 2 LNAzo β.

6.3 System 3

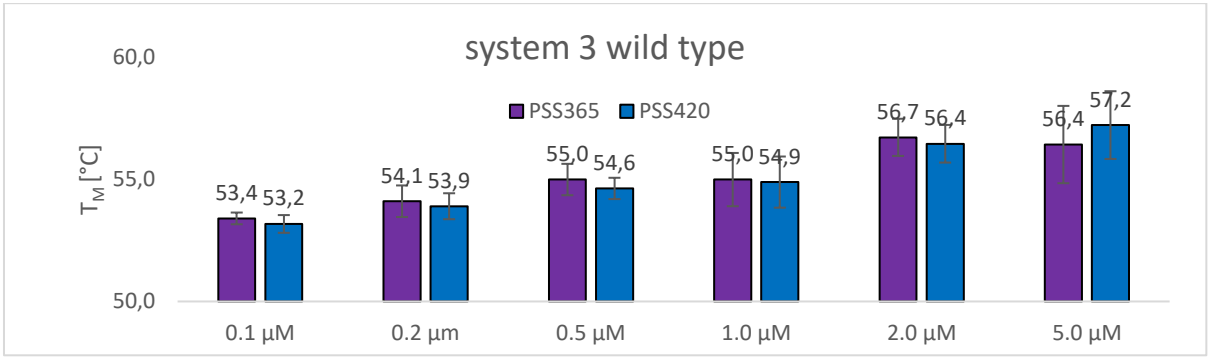

Figure S55: Bar graph of fluorescence-based melting temperatures of system 3 wild type.

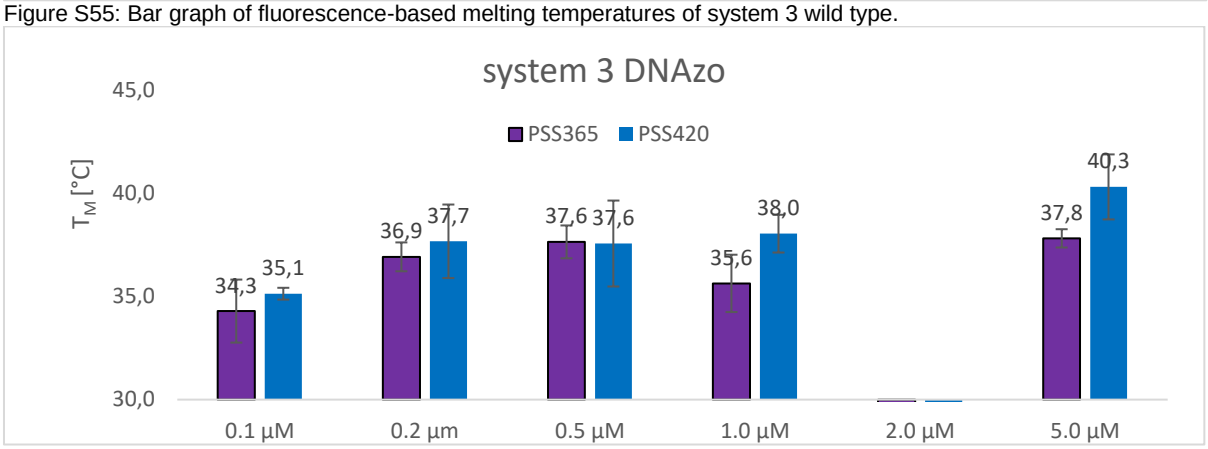

Figure S56: Bar graph of fluorescence-based melting temperatures of system 3 DNAzo.

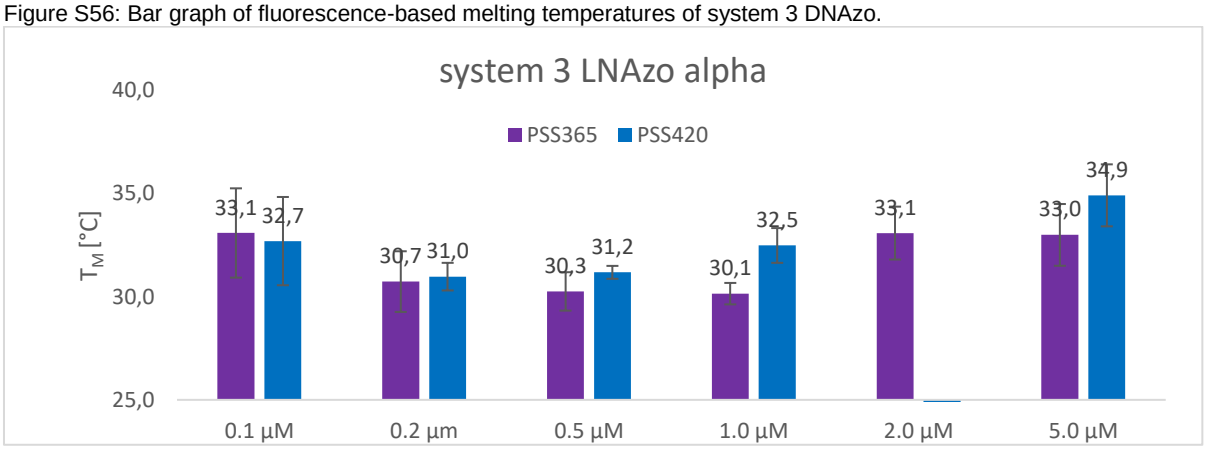

Figure S57: Bar graph of fluorescence-based melting temperatures of system 3 LNAzo α.

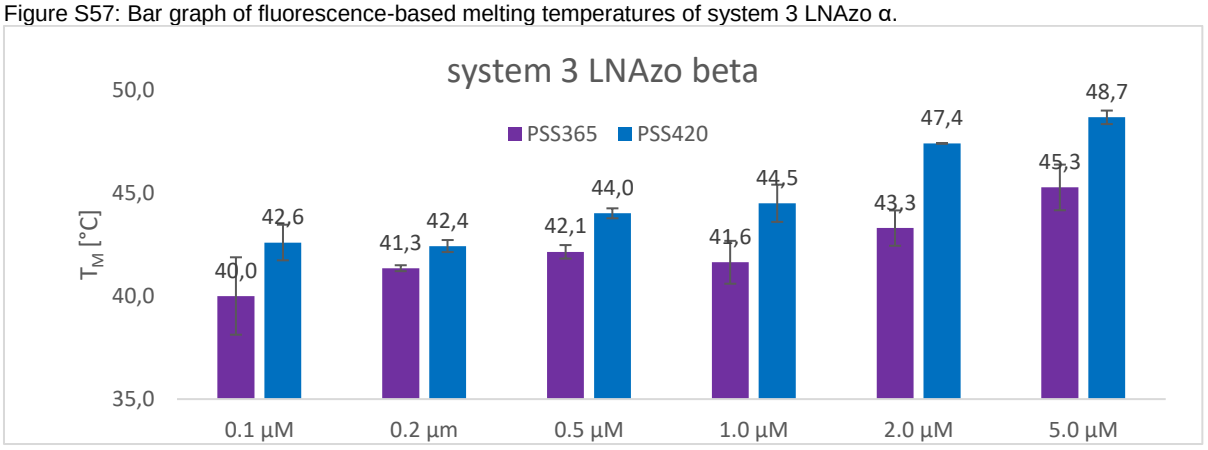

Figure S58: Bar graph of fluorescence-based melting temperatures of system 3 LNAzo β.

6.4 System 4

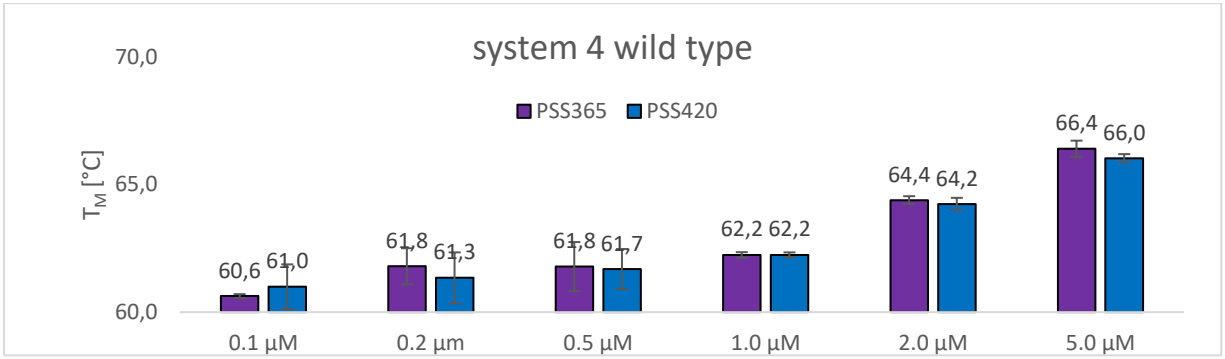

Figure S59: Bar graph of fluorescence-based melting temperatures of system 4 wild type.

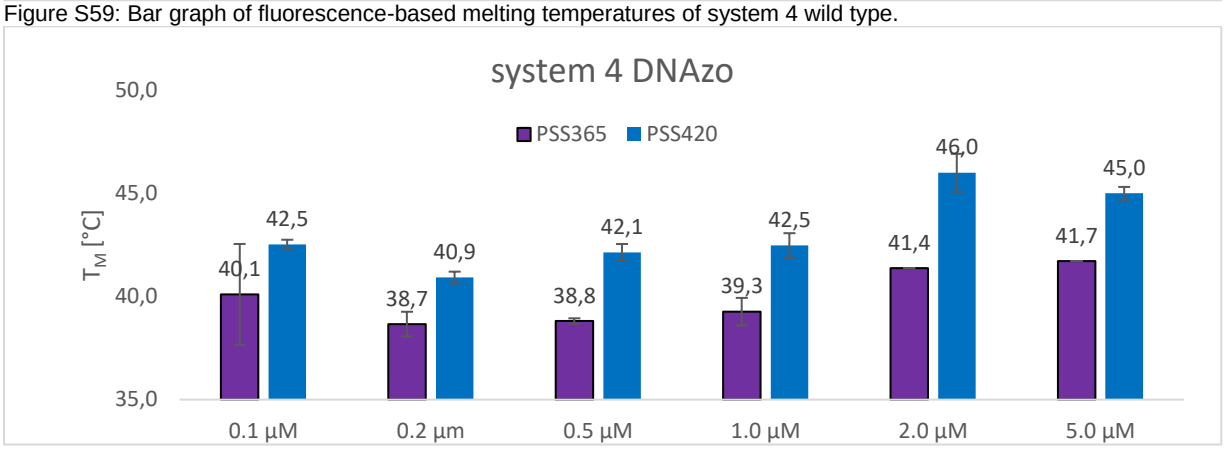

Figure S60: Bar graph of fluorescence-based melting temperatures of system 4 DNAzo.

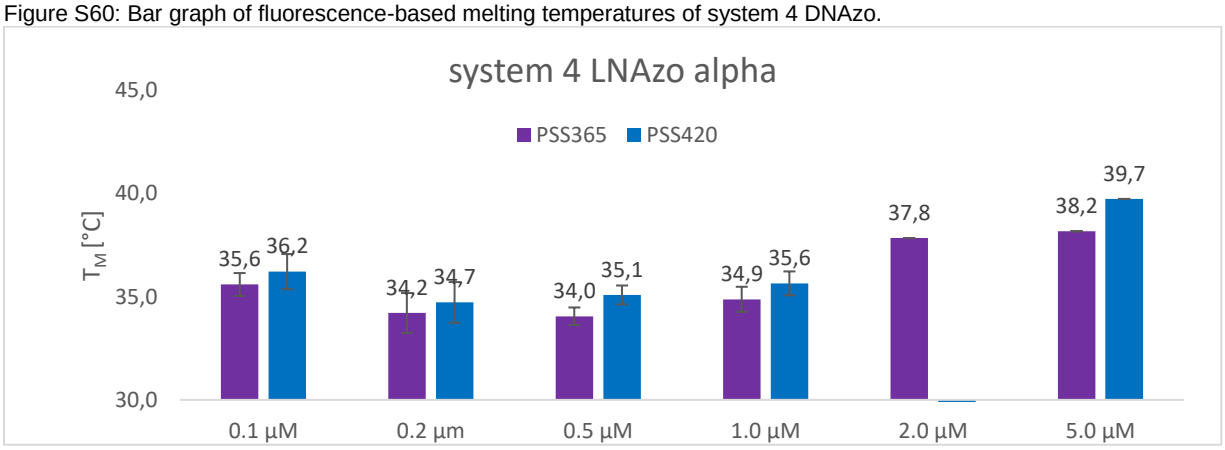

Figure S61: Bar graph of fluorescence-based melting temperatures of system 4 LNAzo α.

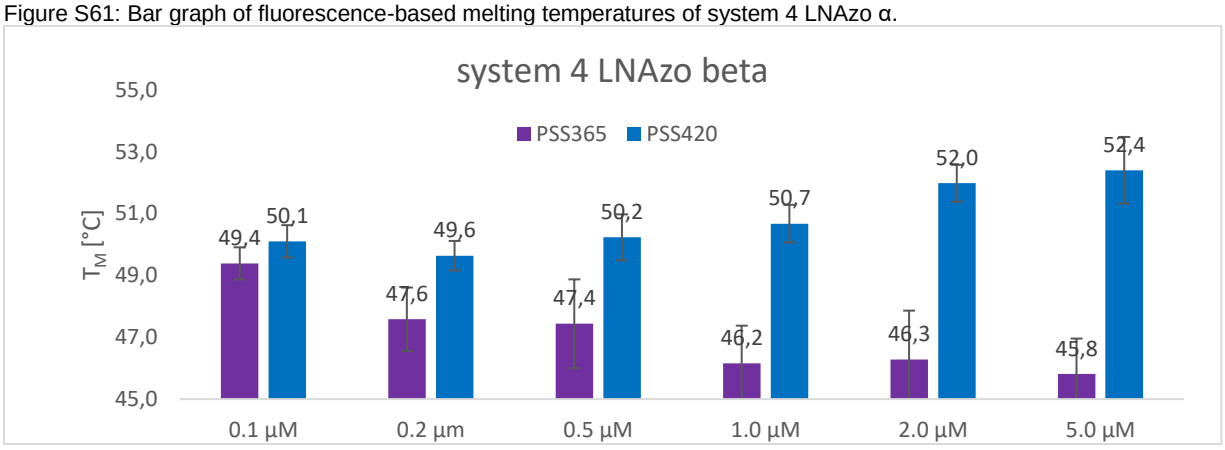

Figure S62: Bar graph of fluorescence-based melting temperatures of system 4 LNAzo β.

7. Influence of the abasic site

To evaluate the influence one abasic site has within a 10mer DNA-duplex, we first measured melting temperatures and CD-spectra of the wild type of system 2 (strand 1+4/2+4, Figure S35b) as used in this study and compared it to the same duplex lacking the terminal fluorophore-quencher pairs (strand 12+13/12+16, Figure S35a). It appears that found results seem to be consistent, with melting temperatures being further decreased, since contribution of the fluorophore-quencher-pair via π-stacking was missing (Figure S36). Also, CD-spectra did show less dominant signals due to decreased helicity (Figure S37+38).

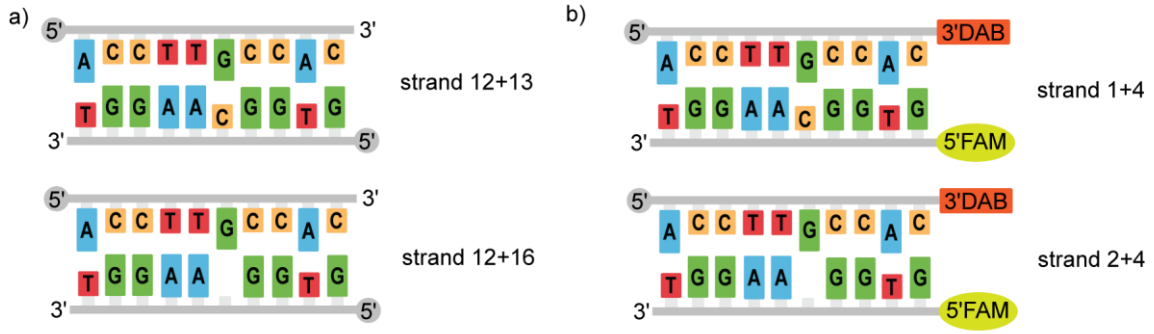

Figure S35: Schematic display of the duplexes used for this study.

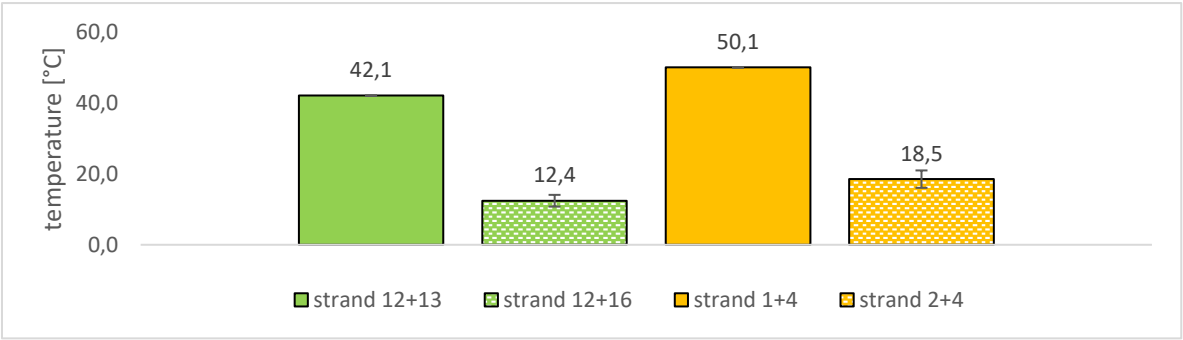

Figure S36: Melting temperatures of the respective duplexes including standard deviation.

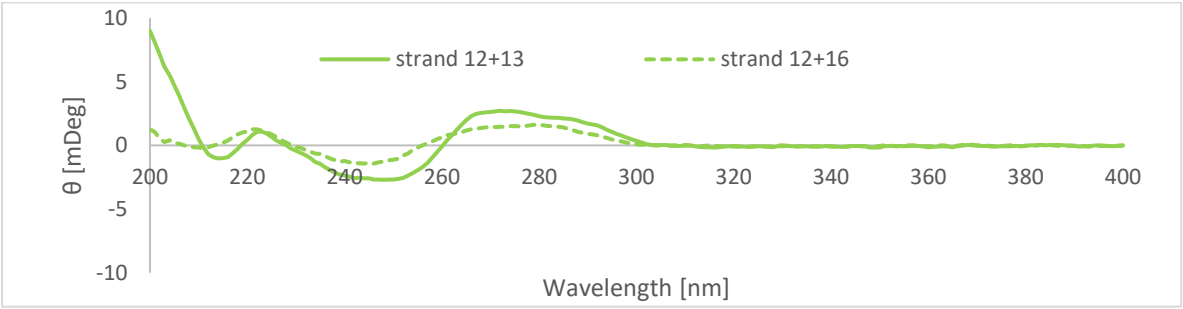

Figure S37: CD-spectra of strands 12+13 compared to strands 12+16.

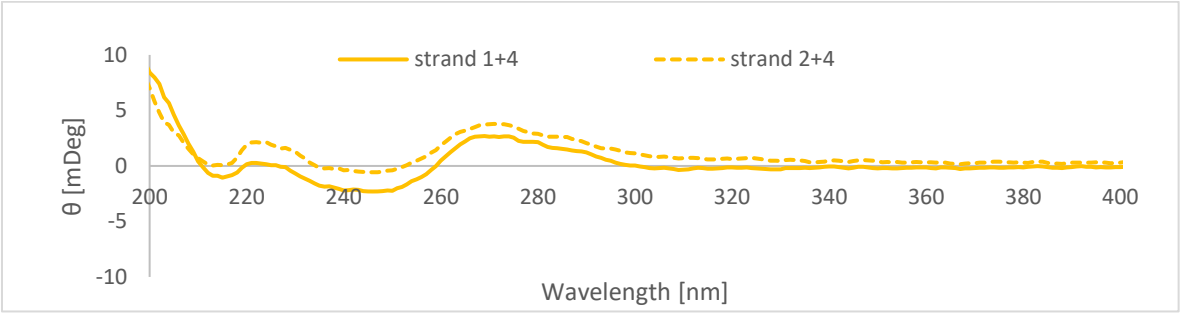

Figure S38: CD-spectra of strands 1+4 compared to strands 2+4.

Furthermore, a permutation of the abasic position within the central bases of the duplex was carried out (Figure S39). Melting temperatures (Figure S40) and CD-spectra (Figure S41) gave further insight into the situation.

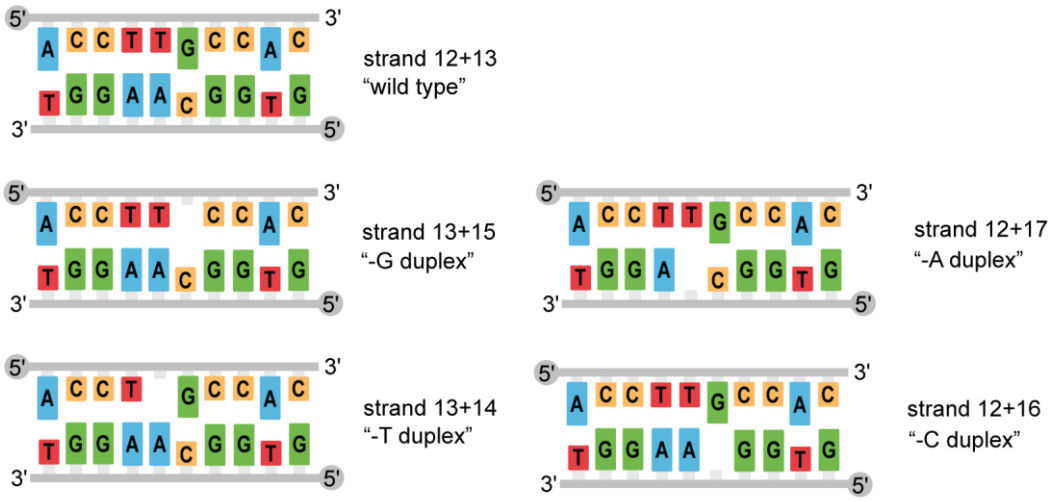

Figure S39: Schematic display of the duplexes used for this study. Duplexes were named after the missing base.

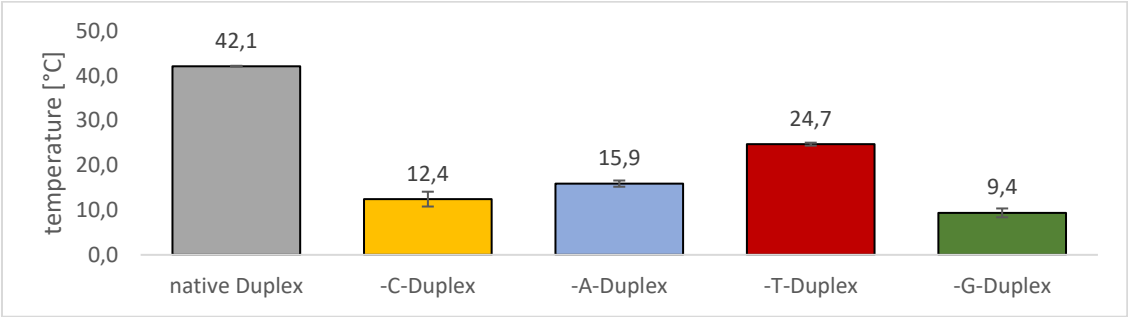

Figure S40: Melting temperatures of described duplexes including standard deviation.

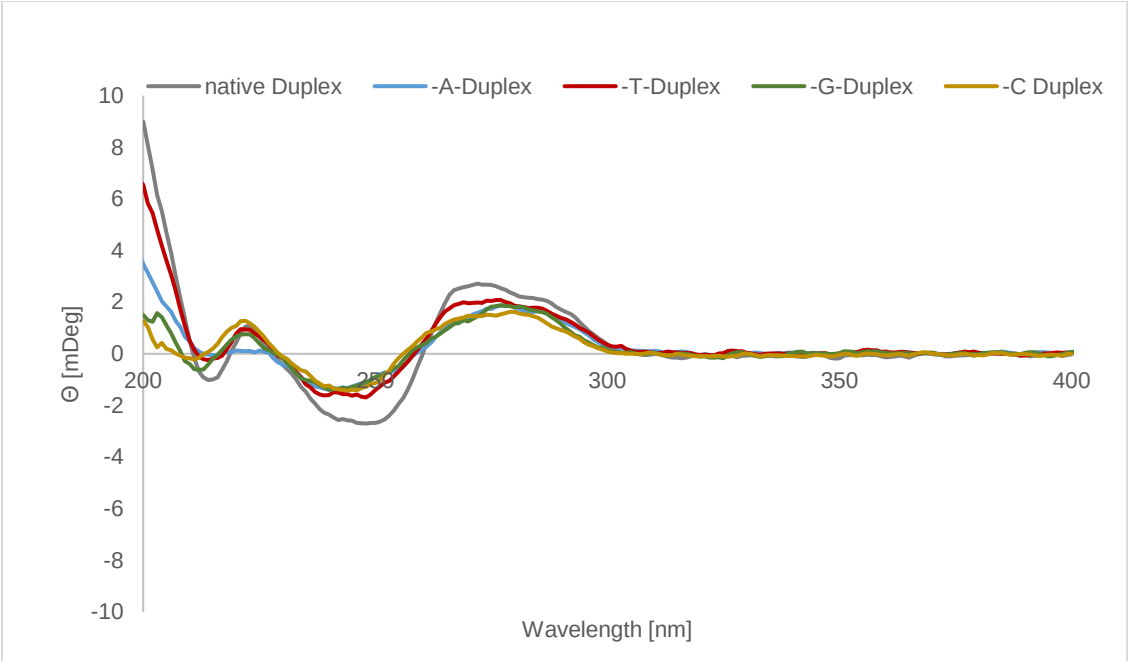

Figure S41: CD-spectra of abasic duplexes.

8. NMR-spectra of synthesized compounds

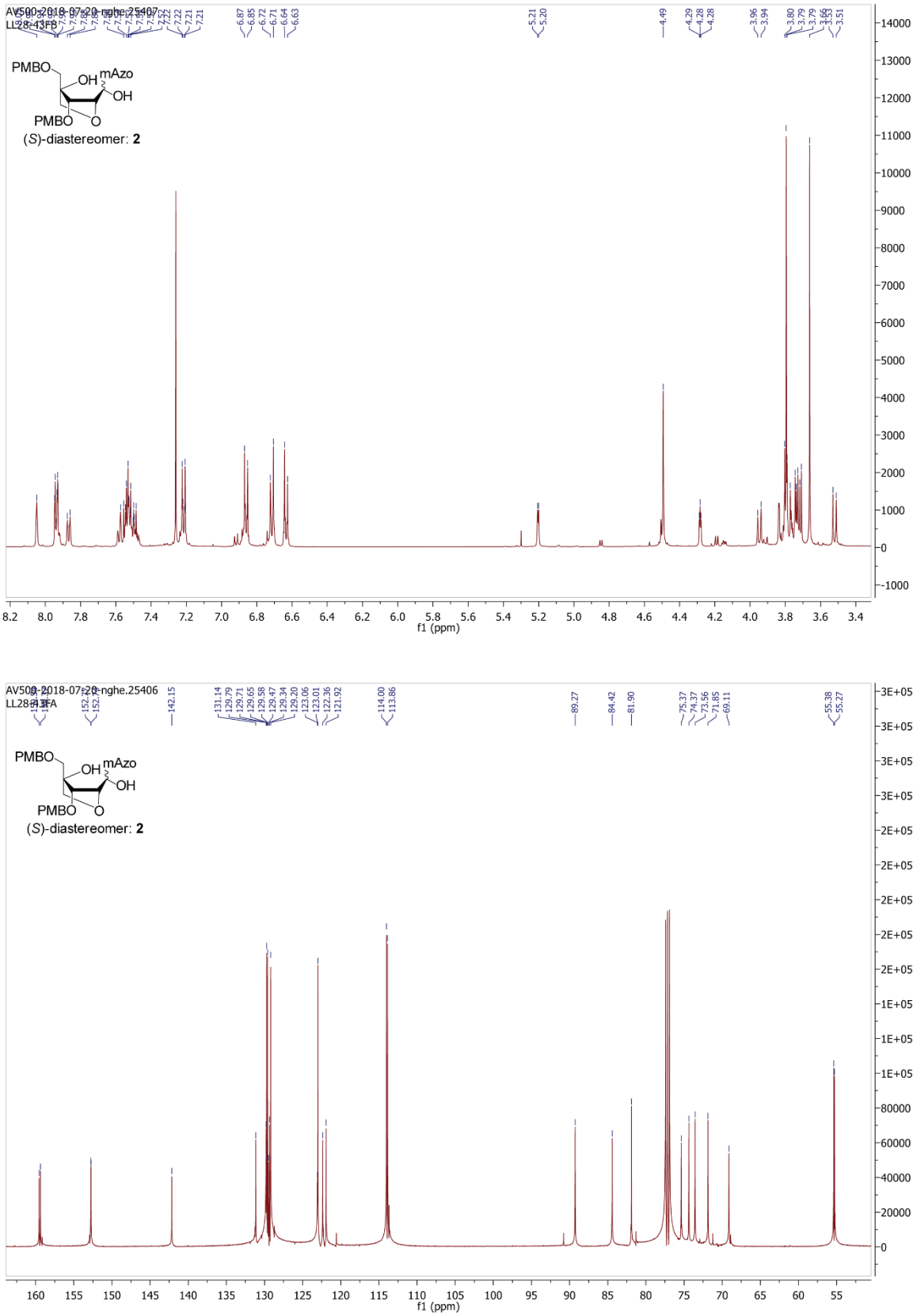

Figure S42: ^{1}H- and ^{13}C-spectrum of compound **2**.

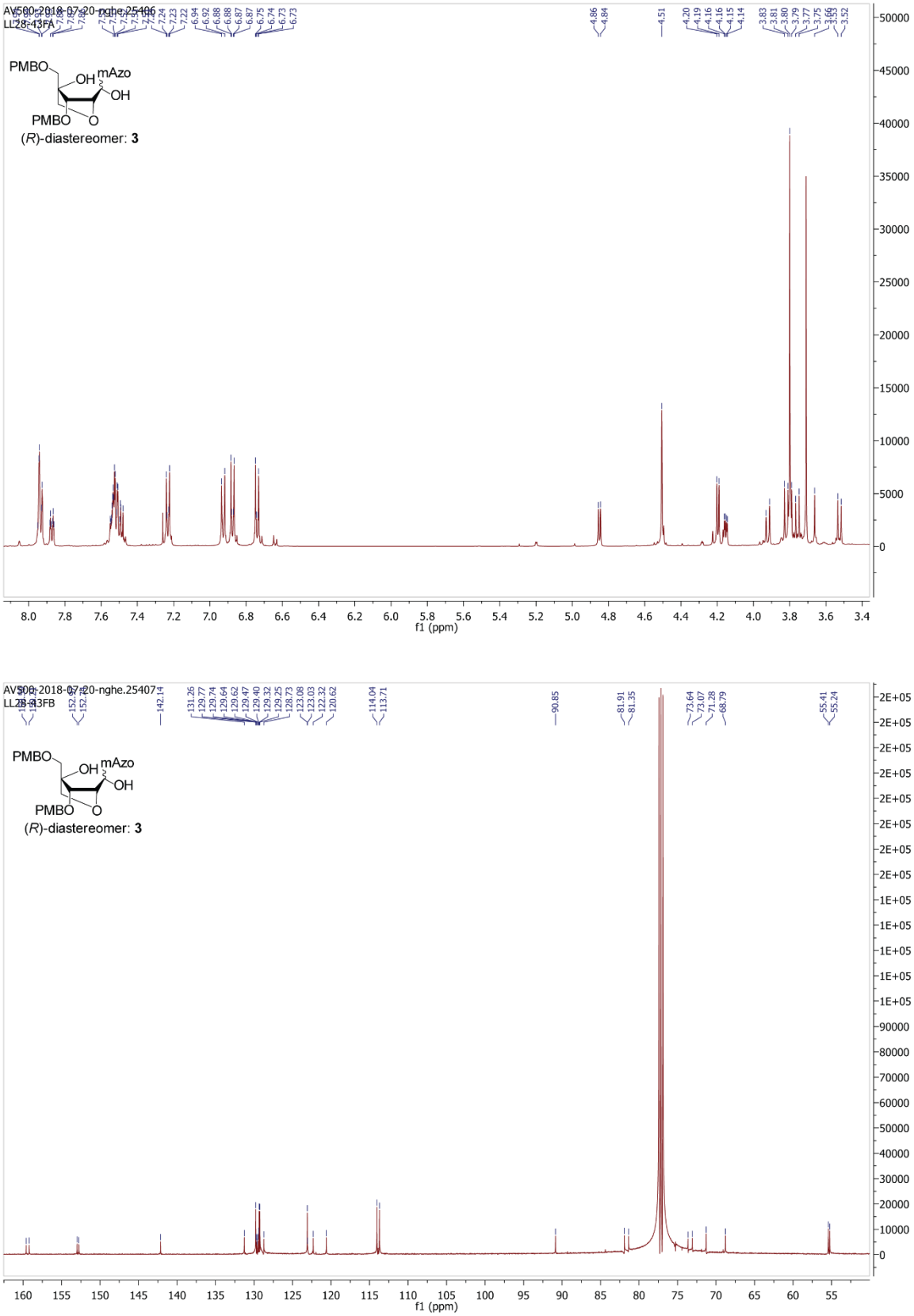

Figure S43: ^{1}H- and ^{13}C-spectrum of compound **3**.

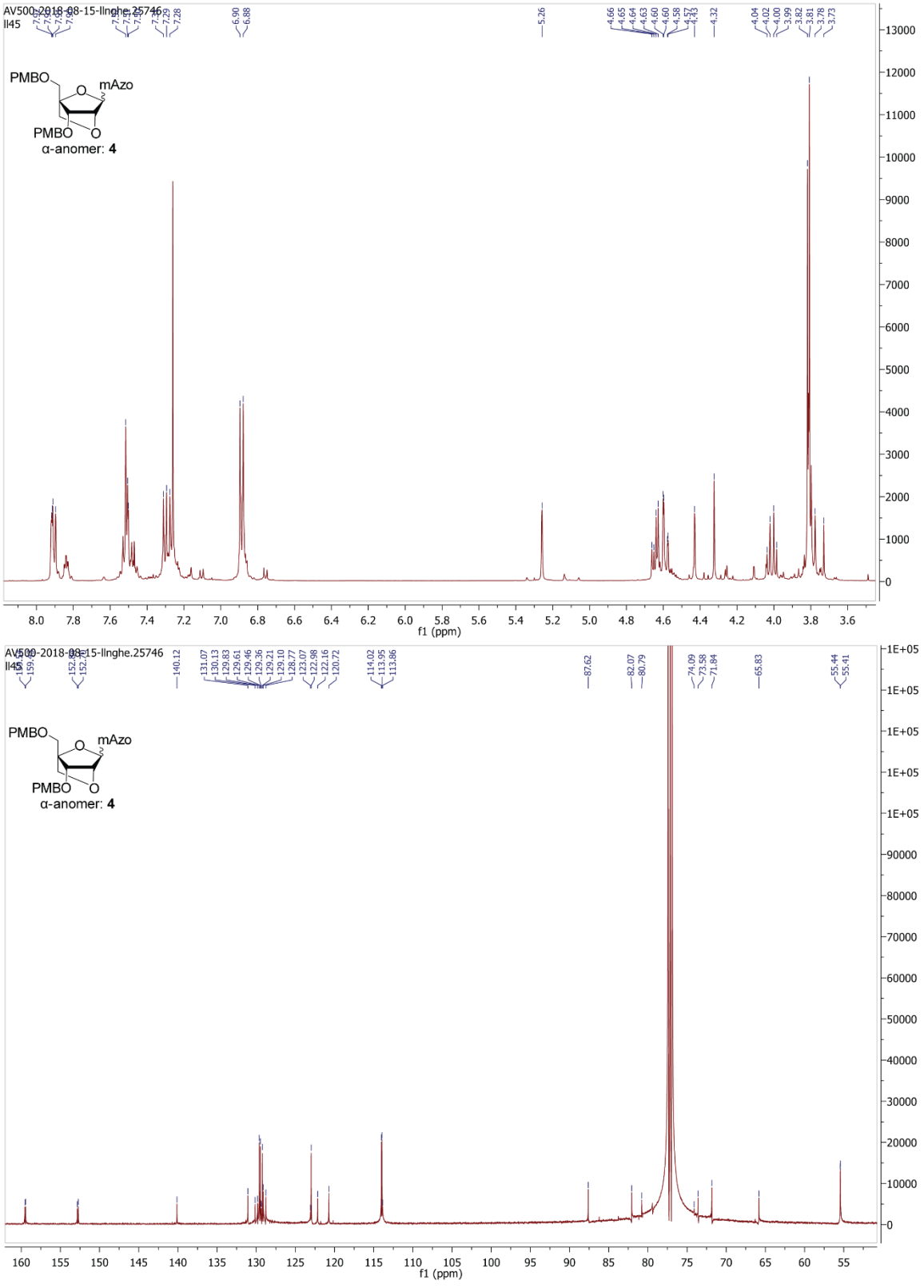

Figure S44: ^{1}H- and ^{13}C-spectrum of compound **4**.

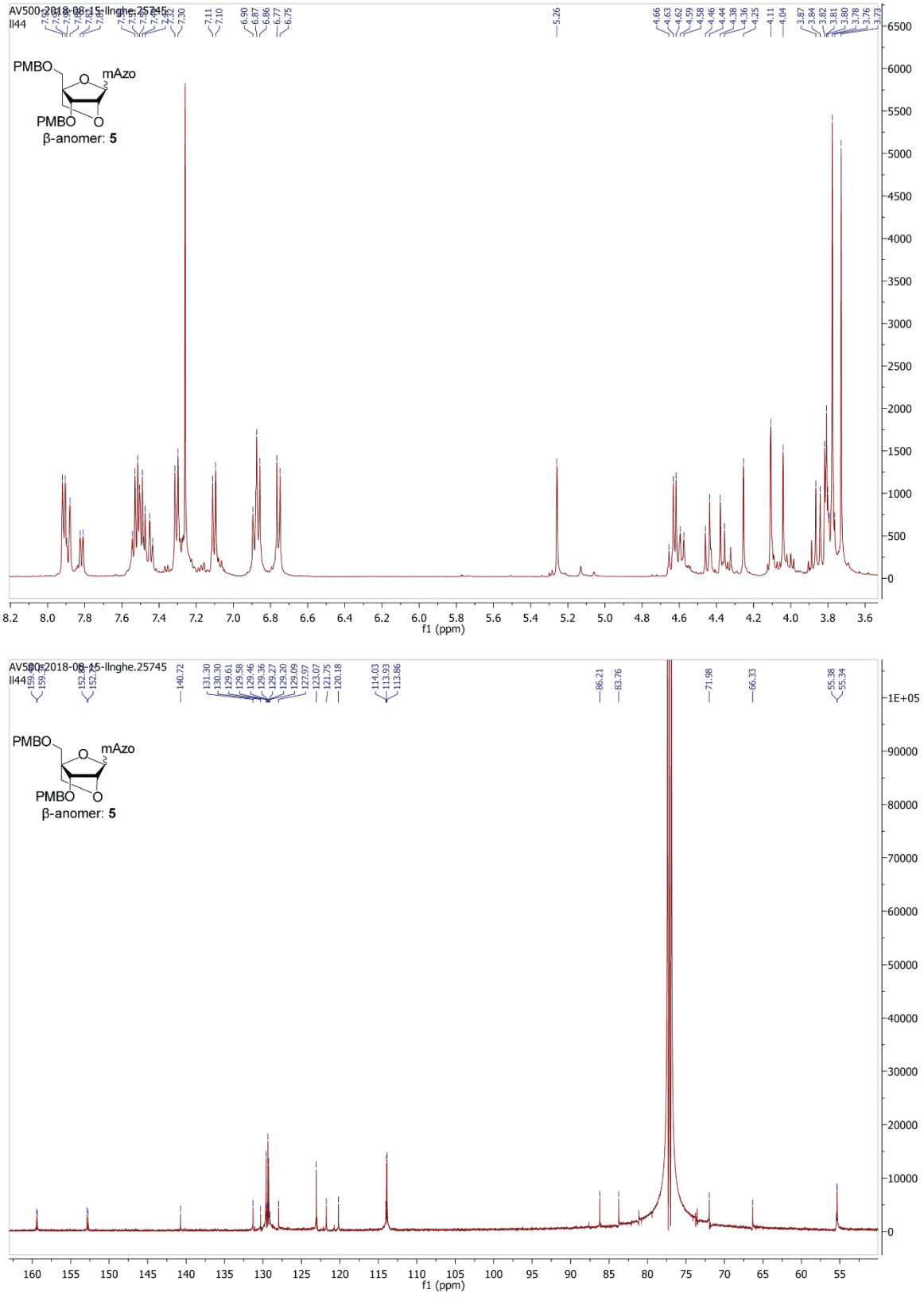

Figure S45: ^{1}H- and ^{13}C-spectrum of compound **5**.

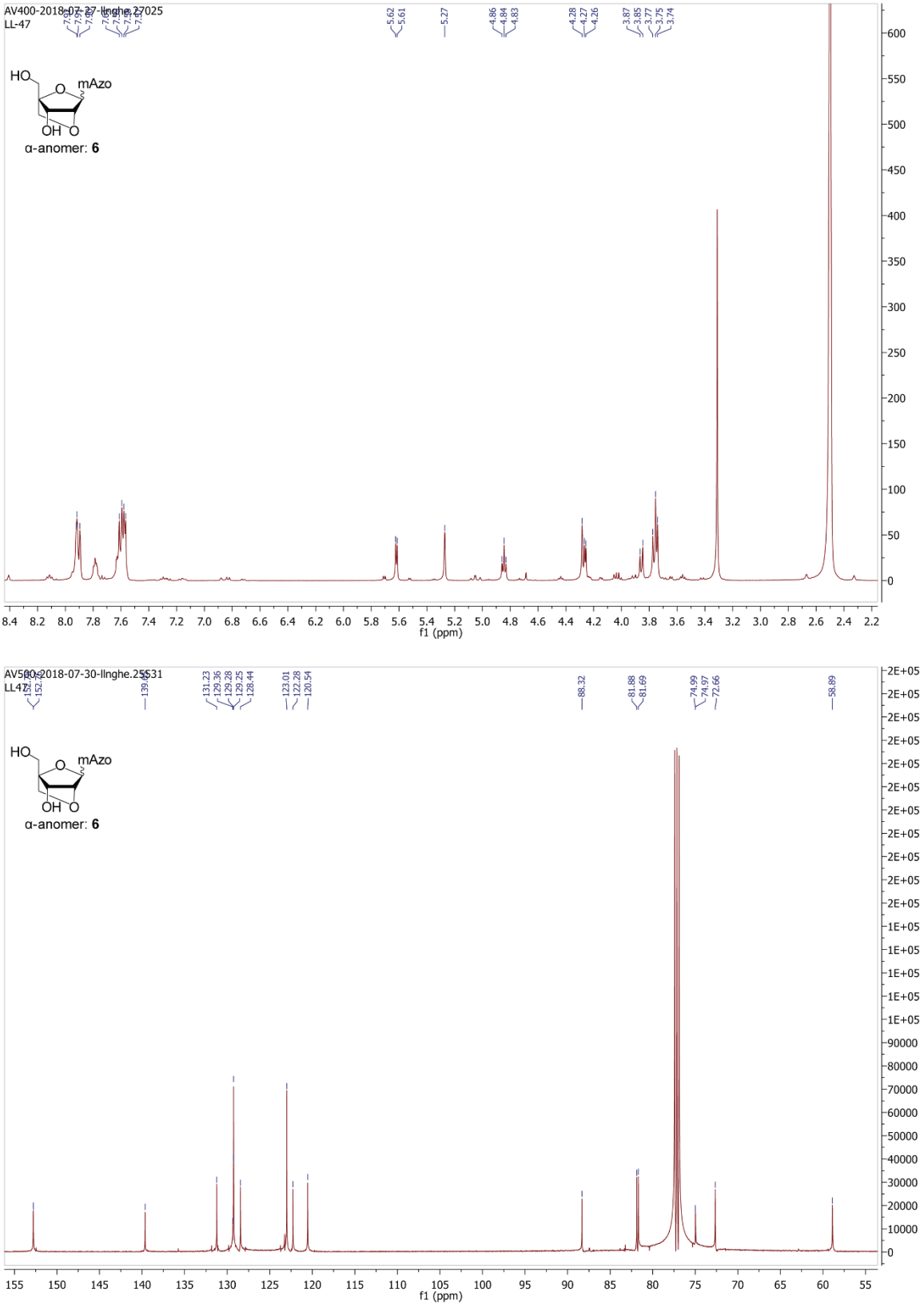

Figure S46: ^{1}H- and ^{13}C-spectrum of compound **6**.

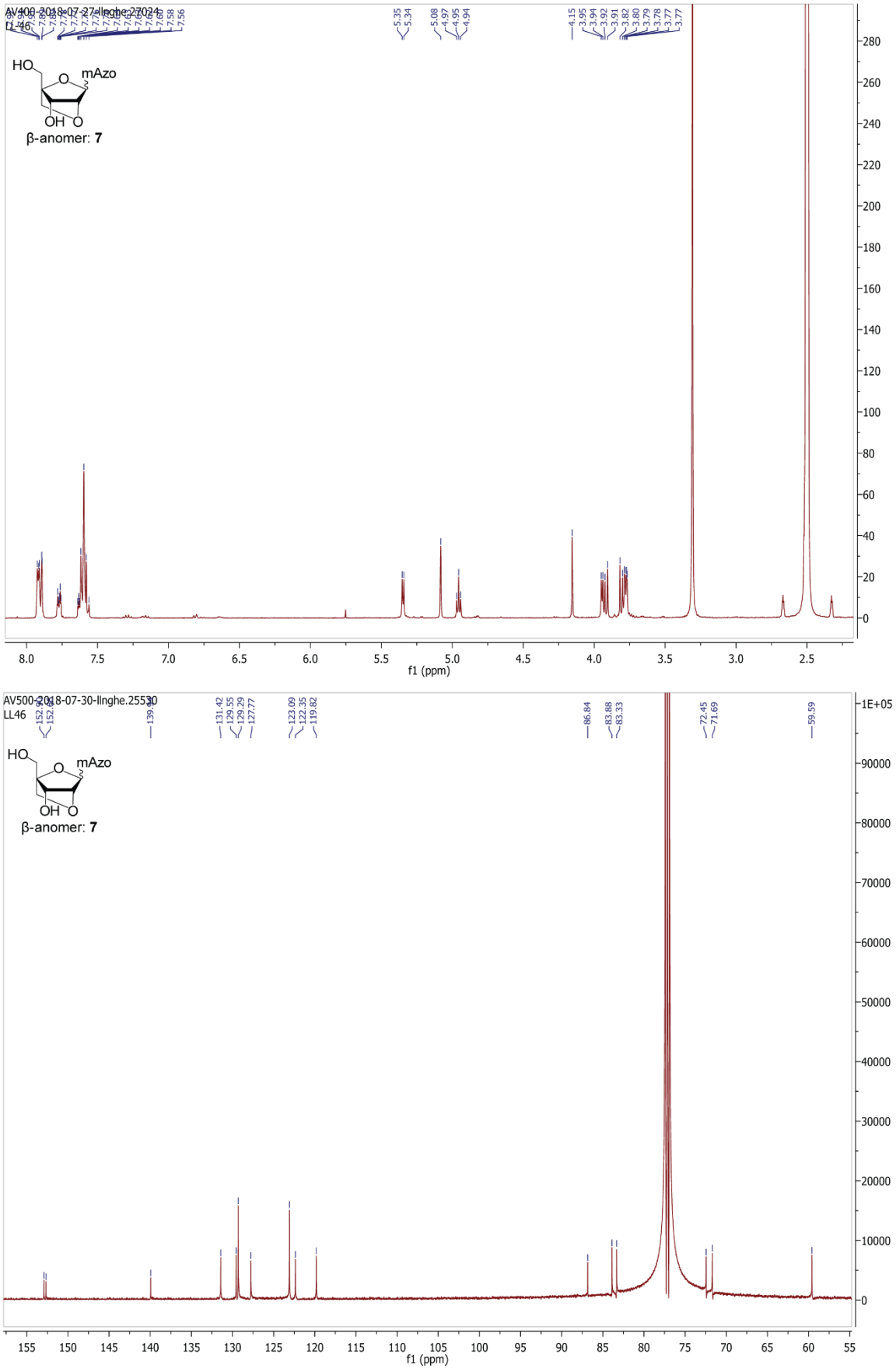

Figure S47: ^{1}H- and ^{13}C-spectrum of compound **7**.

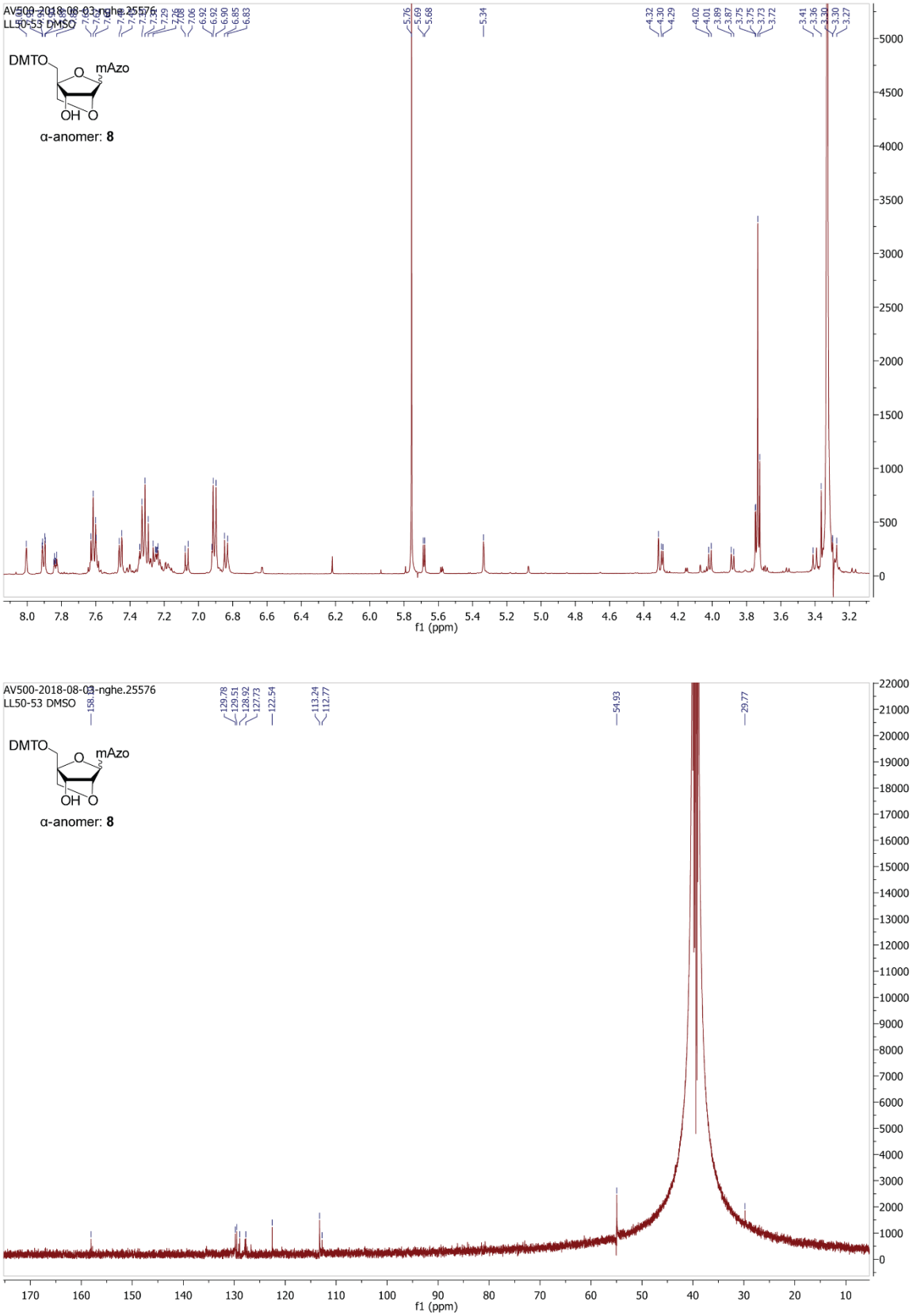

Figure S48: ^{1}H- and ^{13}C-spectrum of compound **8**.

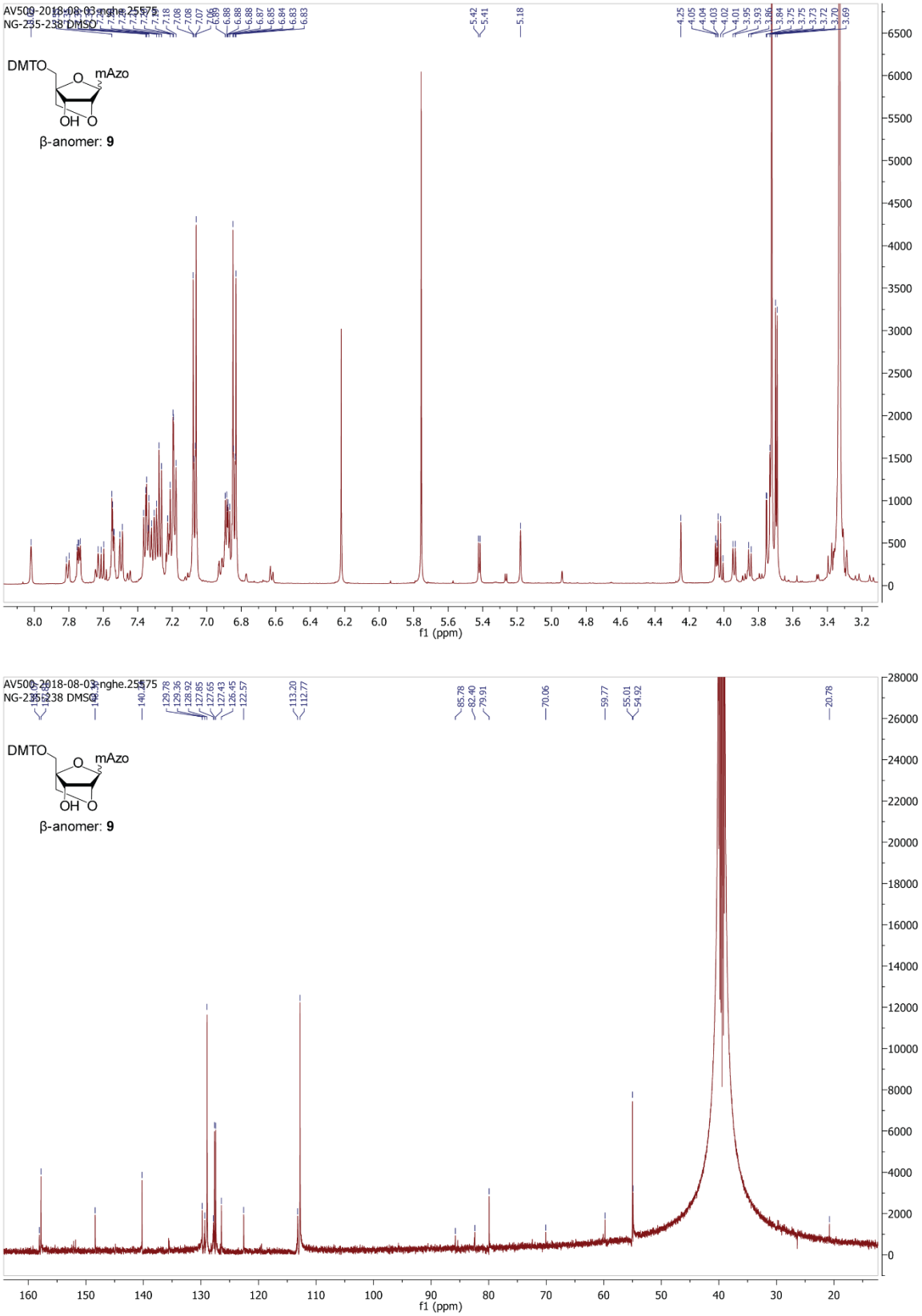

Figure S49: ^{1}H- and ^{13}C-spectrum of compound **9**.

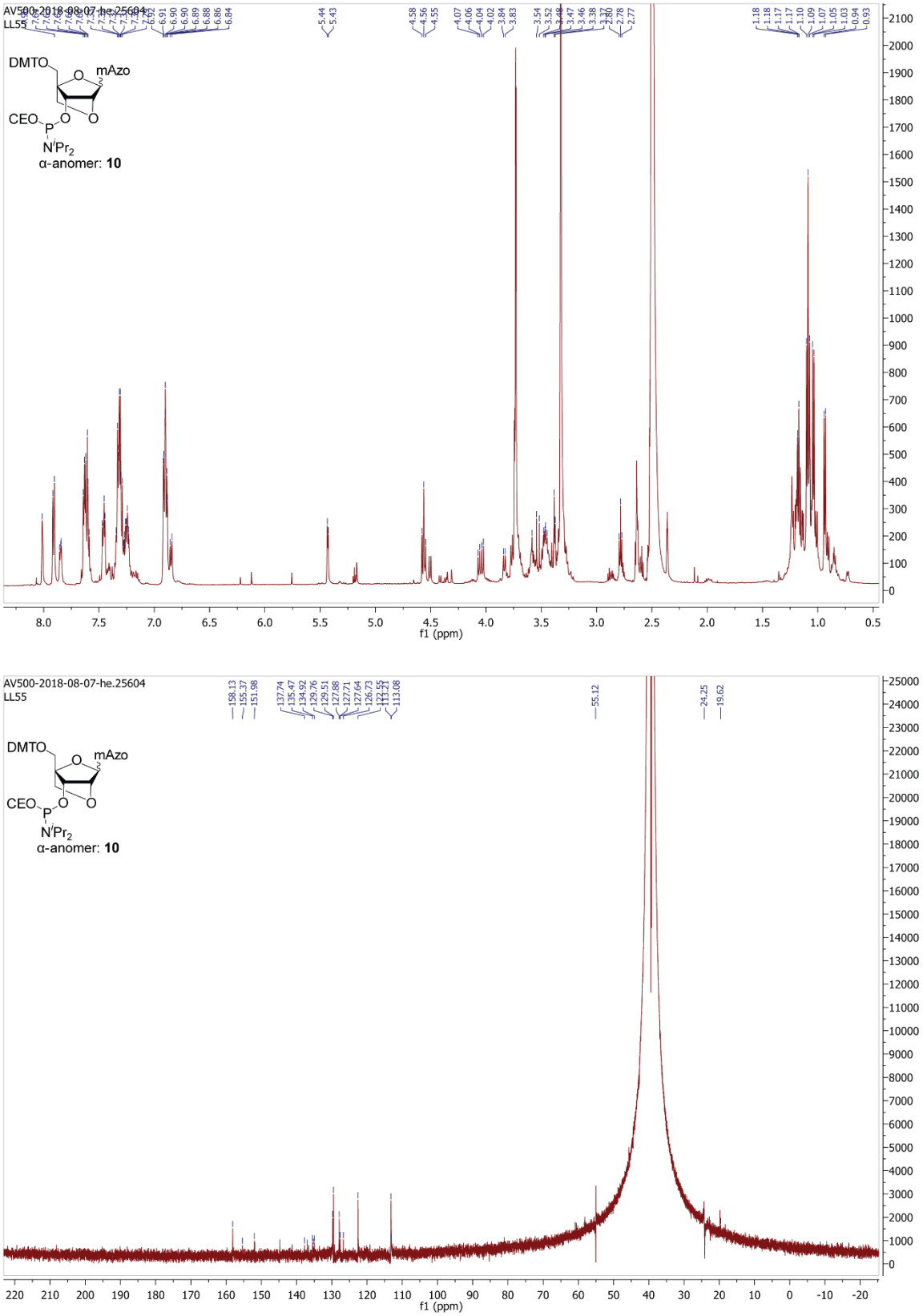

Figure S50: ^{1}H- and ^{13}C-spectrum of compound **10**.

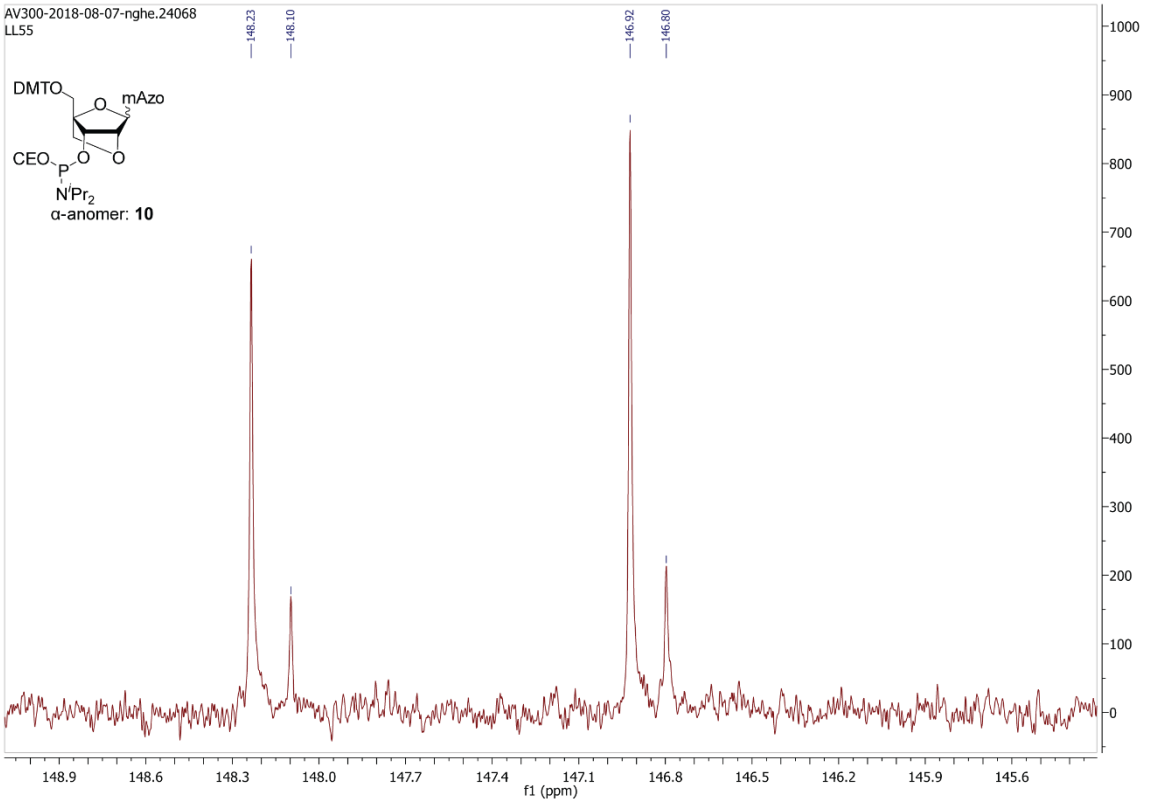

Figure S51: ^{31}P-spectrum of compound **10**.

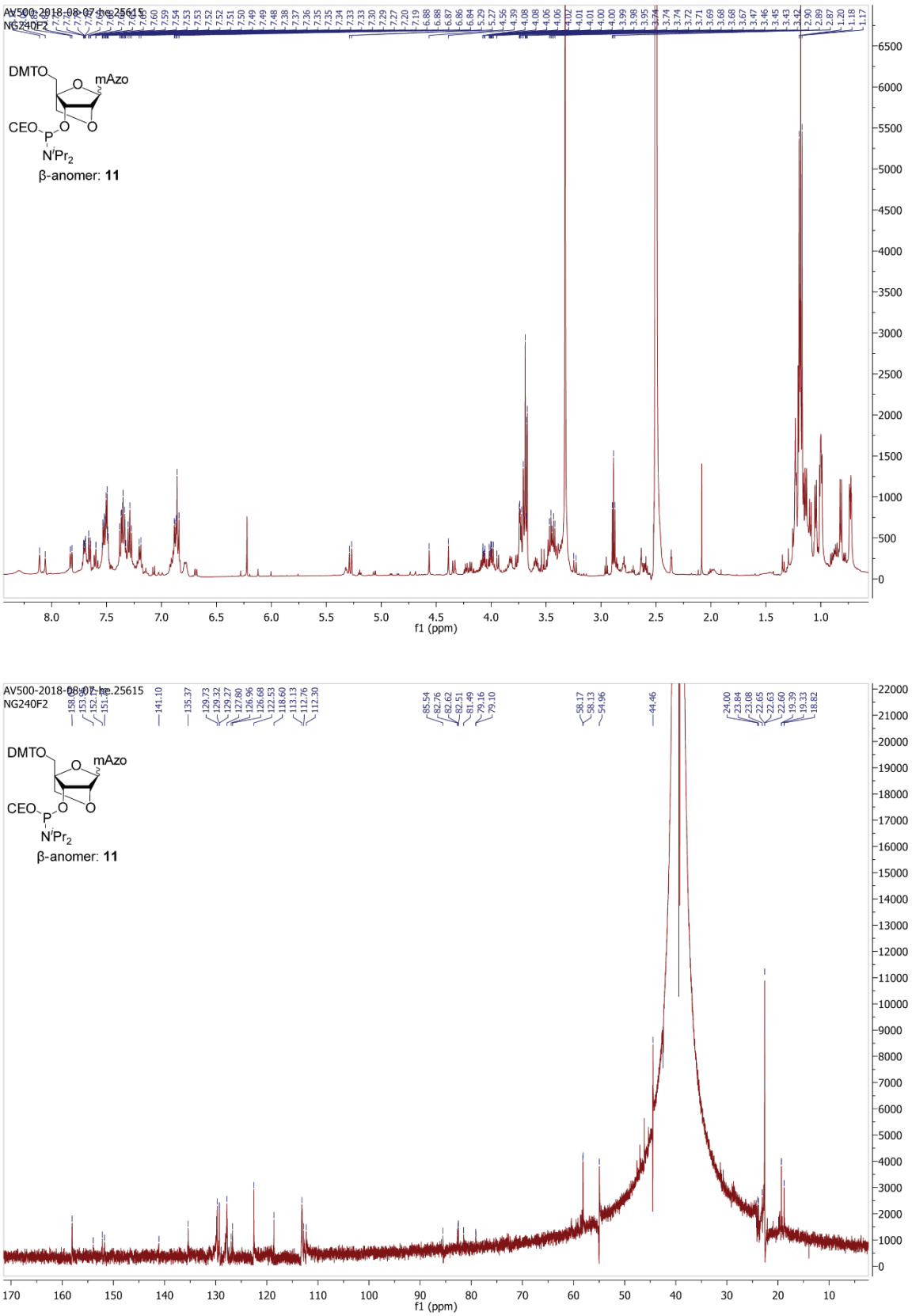

Figure S52: ^{1}H- and ^{13}C-spectrum of compound **11**.

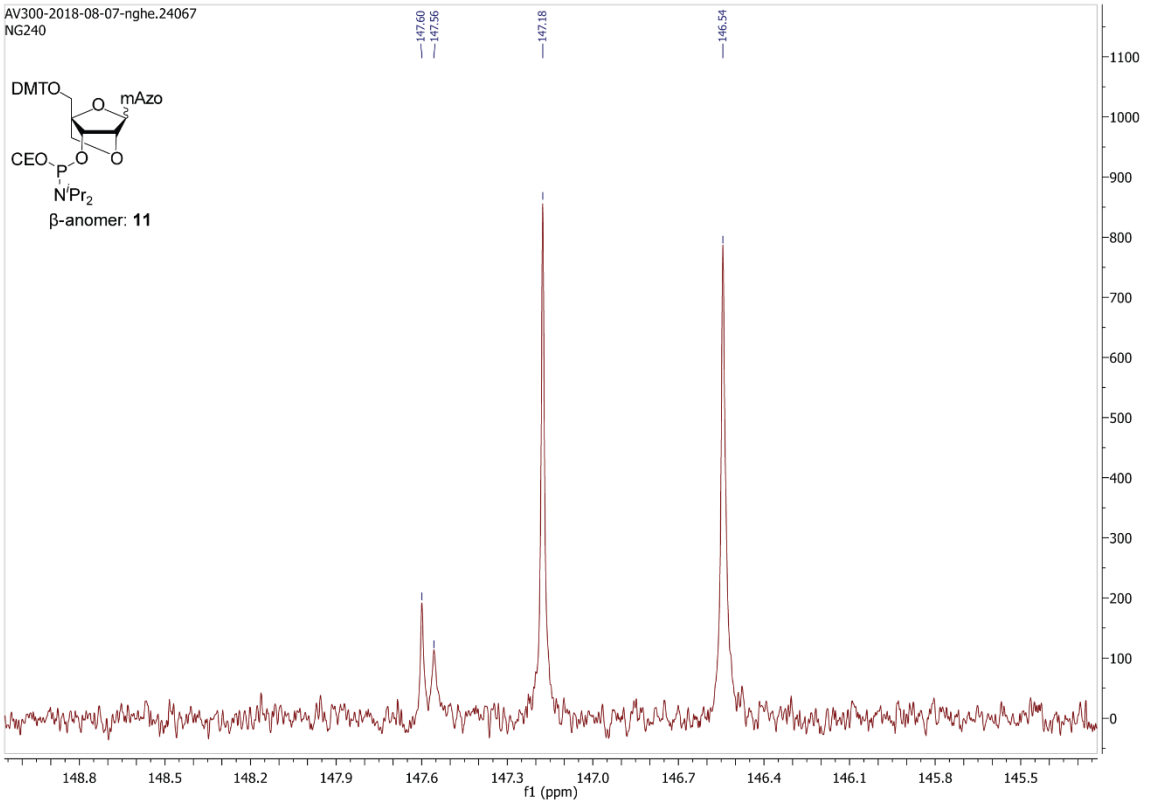

Figure S52: ^{31}P-spectrum of compound **11**.

9. List of abbreviations

Azo	azobenzene
CE	cyanoethyl
Cy	cyclohxane
DAB	3'-dabcyl modification
DCM	dichloromethane
DDQ	2,3-dichloro-5,6-dicyanobenzoquinone
DIPEA	di-*iso*propyl ethyl amine
DNAzo	desoxyribonucleic acid analogue azobenzene *C*-nucleoside
DMT	4,4'-Dimethoxytrityl
EA	ethyl acetate
Et	ethyl
FAM	5' 6-fluorescein modification
Imi	imidazole
LNA	locked nucleic acid
LNAzo	locked nucleic acid analogue azobenzene *C*-nucleoside
Me	methyl
MeOH	methanol
m-Azo	*meta*-azobenzyl
*mi*RNA	*micro*-RNA
^{i}Pr	*iso*propyl
^{n}Bu	*n*-Butyl
PBS	phosphate buffered saline
Ph	phenyl
py	pyridine
PSS	photostationary state (equilibrium state, at which no change of isomeric distribution of a photoswitch occurs anymore during irradiation with a specified wavelength)
PSS365	photostationary state of the azobenzenes at 365 nm wavelength
PSS420	photostationary state of the azobenzenes at 420 nm wavelength
RP-HPLC	reversed phase high performance liquid chromatography
rt	room temperature (25 °C)
*t*Azo	*D*-threoninol-azobenzene
TEA	triethylamine
T_M	melting temperatures (temperature, were the same amount of single stranded and duplex oligonucleotide is present)
TMAD	tetramethylazodicarboxamide